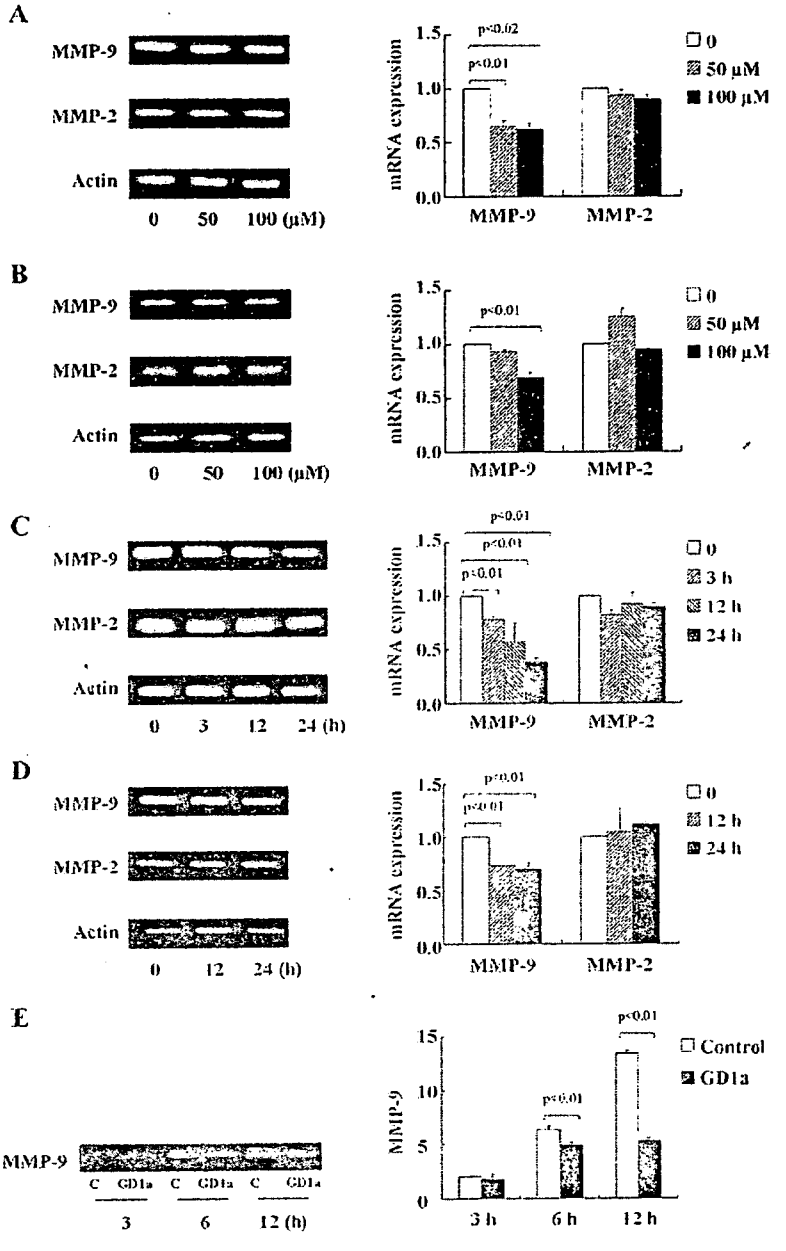

FIG. 3. Effects of exogenous GD1a addition on MMP-9 expression. FBJ-M5 (A) and FBJ-LL (B) cells were incubated with 50 or 100 μM GD1a in the absence of serum for 6 hr and mRNA expression of MMP-9 and MMP-2 was determined. FBJ-M5 (C) and FBJ-LL (D) cells were incubated with 50 μM GD1a in the absence of serum for 3, 12, or 24 hr and mRNA expression of MMPs was determined. FBJ-M5 cells were cultured with or without 50 μM GD1a in the absence of serum for 3, 6, and 12 hr and aliquots were assayed for MMP-9 activity by gelatin zymography (E). Results for densitometric analysis of MMP-9 are shown in the right-hand panel. Two separate determinations were made and standard deviation is given. On the left-hand side of Figures 2A to 2D, representative PCR results are shown.

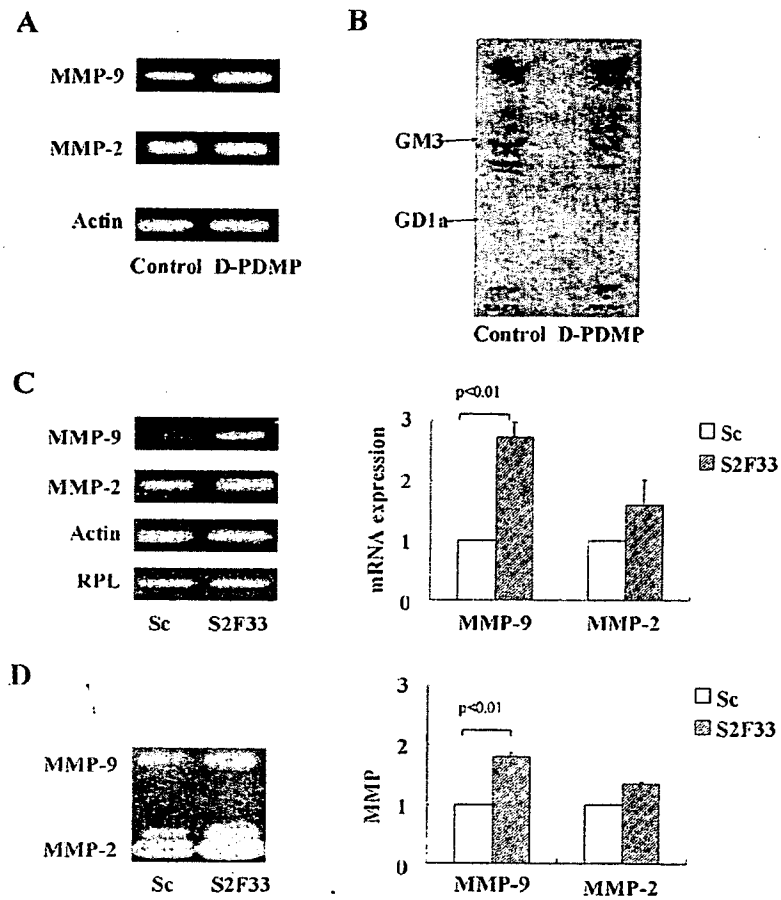

FIG. 4. Increase in MMP-9 expression after GD1a suppression by D-PDMP treatment or siRNA targeting St3gal2 FBJ-M5 cells were cultured with 12.5 μM D-PDMP in complete medium for 6 days and RNA was extracted for analysis of MMPs (A). FBJ-S1 transfected with siRNA targeting St3gal2 or siRNA having the scrambled sequence and monoclonal cell lines showing suppressed expression of St3gal2 were screened by G418. One monoclonal line (S2F33) and control cells (Sc, scrambled sequence) were cultured and glycosphingolipids were analyzed by HPTLC (B). MMPs mRNA expression was assayed (C) and MMP activity by zymography (D). SiRNA targeting St3gal2 transfected cells showed high level of β-actin so that another housekeeping gene, ribosomal protein L13 (RPL), was used as a control in C. In A, C, and D, the left-hand panels show results of RT-PCR or gelatin-zymography and the right-hand panels represent the densitometric analysis.

the levels of all cellular glycosphingolipids. The 12.5 μM D-PDMP treatment did not affect cell viability but suppressed cell proliferation to approximately 60% of controls. Figure 4A shows MMP-9 mRNA of cells treated with D-PDMP for 6 days to be twice that of the control, though there was no change in MMP-2 expression. Lipid fractions of cells treated with D-PDMP contained less than 20% GD1a compared with the control as indicated by HPTLC (Figure 4B).

As an alternative specific approach, FBJ-S1 cells were transfected with siRNA targeting St3gal2 (sialyltransferase responsible for GD1a synthesis, SAT-IV, Siat5). Transiently transfected FBJ-S1 cells, at 3 days transfection, showed suppressed expression of St3gal2 mRNA (75% of the scrambled sequence control) and MMP-9 expression 1.5 times that of the scrambled sequence control (data not shown) and the monoclonal S2F33, obtained by screening transfected cells with G418, expressed MMP-9 by 2.5 times as much (Figure 4C). Figure 4D shows S2F33 cells to produce MMP-9 activity twice that of the control, according to gelatin-zymography. All these findings clearly indicate MMP-9 but not MMP-2 expression to be regulated by GD1a.

DISCUSSION

MMP-9 is known to contribute to the malignant behavior of tumor cells through multiple mechanisms of action [6–8]. The invasion assay utilizing Matrigel-coated membranes is routinely used as a means of assessing cell invasiveness, which correlates

with metastatic potential [17–19]. Inhibitors and the anti-MMP-9 antibody in this study were found to reduce the number of cells invading the membrane. MMP-9 may thus be considered to be a significant factor involved in FBJ cell metastasis. MMP-9 also was found in this study to be negatively regulated by ganglioside GD1a.

Researchers reported in 1996 that in 6 of 8 human glioma cell lines, gangliosides including GD1a upregulate MMP-9 secretion, while in two lines, downregulation was noted [20]. Whether gangliosides are involved in the regulation of MMP-9 transcription remains unknown. Expression of the GD3 synthase gene in vascular smooth muscle cells resulted in inhibition of TNF-alpha-induced MMP-9 expression, according to zymography and immunoblotting [21]. However, whether MMP-9 transcription is affected by introduction of GD3 synthase gene into the muscle cells has yet to be established. Through use of endogenous GM3 expression in keratinocytes, the expression of GM3 has been shown to modulate mRNA expression and enzyme activation of MMP-9 [22]. Neither GM3 overexpression nor ganglioside depletion had any effect on the expression or activity of MMP-9 under conditions of serum, epidermal growth factor, or fibronectin starvation.

Recently, GM1 has been suggested to modulate MMP-9 localization in lipid rafts [23]. Expression levels of GM1 were markedly decreased in the high metastatic lines, whereas MMP-9 levels were significantly increased compared with the control cell line, implying that the increased metastatic activities in the highly metastatic lines depend primarily on the increased secretion and activity of MMP-9 [23]. However, the regulation of MMP-9 expression by GM1 has yet to be clarified.

MMP-9 gene expression is clearly shown in this study to be regulated by GD1a. Three decades ago MMP-9 expression was noted to be high in FBJ-LL cells but low in FBJ-S1 cells [1]. FBJ-LL cells devoid of GD1a synthesize much more MMP-9 than FBJ-S1 cells rich in GD1a. In the transfectant FBJ-5-30 cell produced from a FBJ-LL cell by transfecting GM2/GD2 synthase cDNA, resulting in the same GD1a level as in FBJ-S1 cells, MMP-9 expression was noted to be suppressed. MMP-9 mRNA expression was seen to parallel MMP-9 activity by gelatin zymography. Exogenous addition of GD1a to FBJ-LL or FBJ-M5 cells caused suppression of MMP-9 mRNA and activity. With depletion of GD1a from FBJ-5-30 cells treated with D-PDMP or siRNA targeting St3gal2, MMP-9 mRNA and its activity were noted to increase. MMP-9 of FBJ cells is thus clearly shown to be under the control of GD1a, and the ganglioside GD1a regulation of MMP-9 expression is reported in the present paper for the first time.

Zymography of MMP-9 of FBJ-M5 cells preincubated with GD1a indicated a greater decrease in activity than expected from mRNA suppression. Incubation of conditioned medium containing MMP-9 with GD1a caused MMP-9 activity to decrease. Examination confirmed that MMP-9 activity is actually suppressed and/or MMP-9 protein undergoes degradation by GD1a. GD1a was found to have no effect on MMP-9 activity and Western blots indicated GD1a did not diminish MMP-9 during electrophoresis under reducing conditions. GD1a appeared to mediate the binding of a portion of MMP-9 with certain molecules, with consequently greater molecular mass on the gel, and cause a decrease in the activity of MMP-9 at the site where it would normally appear. Caution should be used in doing gelatin-zymography since molecules other than GD1a may similarly work, causing decrease in MMP-9 activity in zymography. This matter has been reported elsewhere [14].

The exogenous addition of GD1a to FBJ-M5 or FBJ-LL cells suppressed MMP-9 mRNA (Figure 3), while MMP-2 mRNA was not affected by GD1a addition. Whether the effects of exogenous GD1a on MMP-9 expression were exerted by GD1a binding to the putative receptor on the plasma membrane [15] and/or after incorporation to the plasma membrane remains to be elucidated. However, the latter could be the case, since MMP-9 in GD1a-rich cells such as FBJ-S1 and -LA5-30 cells was low in the expression compared with GD1a-less FBJ-M5 and -LL cells.

Whether suppresion of MMP-9 by GD1a is specific to this particular ganglioside has yet to be addressed, as a relationship between GM1 expression and MMP-9 suppression has been suggested [23]. Moreover, whether GD1a *per se* is the actual regulatory molecule remains to be determined. The functional glycosphingolipid may possibly be situated downstream from GD1a, either as a product with much greater or less carbohydrate content or which perhaps undergoes O-acylation or another derivitization. However, GD1a could be the actual regulatory molecule responsible as there is a precedent in other systems.

Gangliosides may bind to and regulate the epidermal growth factor receptor [24], neurite growth factor receptor Trk [25], and calmodulin [26]. Gangliosides bind to and regulate calmodulin-dependent enzymes [26, 27]. In interactions with phosphodiesterase, gangliosides at low concentration activate calmodulin-dependent enzymes by binding to molecules at the calmodulin-binding site, and at higher concentrations, they inhibit enzymes by binding to calmodulin-like sites [28]. GT1b has been shown to have greater affinity toward calmodulin-binding sites of phosphodiesterase, followed by GD1a, GD1b, and GM1a. Thus, GD1a may reasonably be considered a candidate should GD1a bind to molecules involved in signal transduction in FBJ cells. Clarification of the mechanism by which GD1a regulates caveolin-1, Stim1, and MMP-9 gene expression is currently in progress.

ACKNOWLEDGEMENTS

The authors are grateful to Dr. Frances M. Platt (Department of Pharmacology, University of Oxford) for her critical reading of the manuscript.

REFERENCES

1. Yamagata, S., Tanaka, R., Ito, Y., and Shimizu, S. (1989). Gelatinase of murine metastatic tumor cells. *Biochem. Biophys. Res. Commun.*, 158, 228–234.

2. Curran, S., and Murray, G.I. (2000). Matrix metalloproteinases: molecular aspects of their roles in tumour invasion and metastasis. *Eur. J. Cancer*, 36, 1621–1630.
3. Klein, G., Vellenga, E., Fraaije, M.W., Kamps, W.A., and de Bont, E.S.J.M. (2004). The possible role of matrix metalloproteinase (MMP)-2 and MMP-9 in cancer, e.g. acute leukemia. *Crit. Rev. Oncol/Hematol*, 50, 87–100.
4. Rundhaug, J.E. (2005). Matrix metalloproteinases and angiogenesis. *J. Cell. Mol. Med.*, 9, 267–285.
5. Liotta, L.A., and Stetler-Stevenson, W.G. (1991). Tumor invasion and metastasis: an importance of positive and negative regulation. *Cancer Res.* 51, 5054–5059.
6. Kaplan, R.N., Riba, R.D., Zacharoulis, S., Bramley, A.H., Vincent, L., Costa, C., MacDonald, D.D., Jin, D.K., Shido, K., Kerns, S.A., Zhu, Z.P., Hicklin, D., Wu, Y., Port, J.L., Altorki, N., Port, E.R., Ruggero, D., Shmelkov, S.V., Jensen, K.K., Rafii, S., and Lyden, S.D. (2005). VEGFR1-positive haematopoietic bone marrow progenitors initiate the pre-metastatic niche. *Nature*, 438, 820–827.
7. Freije, J.M., Balbin, M., Pendas, A.M., Sanchez, L.M., Puente, X.S., and Lopez-Otin, C. (2003). Matrix metalloproteinases and tumor progression. *Adv. Exp. Med. Biol.*, 532, 91–107.
8. Fridman, R., Toth, M., Chvyrkova, I., Meroueh, S.O., and Mobashery, S. (2003). Cell surface association of matrix metalloproteinase-9 (gelatinase B). *Cancer Metast. Rev.*, 22, 153–166.
9. Hakomori, S., and Igarashi, Y. (1995). Functional role of glycosphingolipids in cell recognition and signaling. *J. Biochem. (Tokyo)*, 118, 1091–103.
10. Hakomori, S. (1986). Tumor-associated glycolipid antigens, their metabolism and organization. *Chem. Phys. Lipids*, 42, 209–33.
11. Hyuga, S., Yamagata, S., Tai, T., and Yamagata, T. (1997). Inhibition of highly metastatic FBJ-LL cell migration by ganglioside GD1a highly expressed in poorly metastatic FBJ-S1 cells. *Biochem. Biophys. Res. Commun.*, 231, 340–343.
12. Hyuga, S., Yamagata, S., Takatsu, Y., Hyuga, M., Nakanishi, H., Furukawa, K., and Yamagata, T. (1999). Suppression of FBJ-LL cell adhesion to vitronectin by ganglioside GD1a and loss of metastatic capacity. *Int. J. Cancer*, 83, 685–691.
13. Wang, L., Takaku, S., Wang, P., Hu, D., Hyuga, S., Sato, T., Yamagata, S., and Yamagata, T. (2006). Ganglioside GD1a regulation of caveolin-1 and stim1 expression in mouse. FBJ cells: augmented expression of caveolin-1 and Stim1 in cells with increased GD1a content. *Glycoconj. J.*, 23, 303–315.
14. Hu, D., Tan, X., Sato, T., Yamagata, S., and Yamagata, T. (2006). Apparent suppression of MMP-9 activity by GD1a as determined by gelatin zymography. *Biochem. Biophys. Res. Commun.*, 349, 426–431.
15. Chen, N., Furuya, S., Doi, H., Hashimoto, Y., Kudo, Y., and Higashi, H. (2003). Ganglioside/calmodulin kinase II signal inducing cdc42-mediated neuronal actin reorganization. *Neuroscience*, 120, 163–176.
16. Inokuchi, J., and Radin, N.S. (1987). Preparation of the active isomer of 1-phenyl-2-decanoylamino-3-morpholino-1-propanol, inhibitor of murine glucocerebroside synthetase. *J. Lipid Res.*, 28, 565–71.
17. Hazan, R.B., Phillips, G.R., Qiao, R.F., Norton, L., and Aaronson, S.A. (2000). Exogenous expression of N-cadherin in breast cancer cells induces cell migration, invasion, and metastasis. *J. Cell Biol.*, 148, 779–790.
18. Kim, J.R., and Kim, C.H. (2004). Association of a high activity of matrix metalloproteinase-9 to low levels of tissue inhibitors of metalloproteinase-1 and -3 in human hepatitis B-viral hepatoma cells. *Int. J. Biochem. Cell Biol.*, 36, 2293–2306.
19. Williams, T.M., Medina, F., Badano, I., Hazan, R.B., Hutchinson, J., Muller, W.J., Chopra, N.G., Scherer, P.E., Pestell, R.G., and Lisanti, M.P. (2004). Caveolin-1 gene disruption promotes mammary tumorigenesis and dramatically enhances lung metastasis in vivo. Role of Cav-1 in cell invasiveness and matrix metalloproteinase (MMP-2/9) secretion. *J. Biol. Chem.*, 279, 51630–51646.
20. Maidment, S.L., Merzak, A., Koochekpour, S., Rooprai, H.K., Rucklidge, G.J., and Pilkington, G.J. (1996). The effect of exogenous gangliosides on matrix metalloproteinase secretion by human glioma cells in vitro. *Eur. J. Cancer*, 32A, 868–871.
21. Moon, S.K., Kim, H.M., Lee, Y.C., and Kim, C.H. (2004). Disialoganglioside (GD3) synthase gene expression suppresses vascular smooth muscle cell responses via the inhibition of ERK1/2 phosphorylation, cell cycle progression, and matrix Metalloproteinase-9 expression. *J. Biol. Chem.*, 279, 33063–33070.
22. Xang, Q.W., Sun, P., and Paller, A.S. (2003). Ganglioside GM3 inhibits matrix metalloproteinase-9 activation and disrupts its association with integrin. *J. Biol. Chem.*, 278, 25591–25599.
23. Zhang, Q., Furukawa, K., Chen, H.H., Sakakibara, T., Urano, T., and Furukawa, K. (2006). Metastatic potential of mouse Lewis lung cancer cells is regulated via ganglioside GM1 by modulating the matrix metalloprotease-9 localization in lipid rafts. *J. Biol. Chem.*, 281, 18145–18155.
24. Miljan, E.A., Meuillet, E.J., Mania-Farnell, B., George, D., Yamamoto, H., Simon, H.G., and Bremer, E.G. (2002). Interaction of the extracellular domain of the epidermal growth factor receptor with gangliosides. *J. Biol. Chem.*, 277, 10108–10113.
25. Mutoh, T., Tokuda, A., Miyadai, T., Hamaguchi, M., and Fujiki, N. (1995). Ganglioside GM1 binds to the Trk protein and regulates receptor function. *Proc. Natl. Acad. Sci. USA*, 92, 5087–5091.
26. Higashi, H., Omori, A., and Yamagata, T. (1992). Calmodulin, a ganglioside-binding protein. Binding of gangliosides to calmodulin in the presence of calcium. *J. Biol. Chem.*, 267, 9831–9838.
27. Higashi, H., and Yamagata, T. (1992). Mechanism for ganglioside-mediated modulation of a calmodulin-dependent enzyme. Modulation of calmodulin-dependent cyclic nucleotide phosphodiesterase activity through binding of gangliosides to calmodulin and the enzyme. *J. Biol. Chem.*, 267, 9839–9843.
28. Higashi, H., Yoshida, S., Sato, K., and Yamagata, T. (1996). Interaction of ganglioside with specific peptide sequences as a mechanism for the modulation of calmodulin-dependent enzymes. *J. Biochem. (Tokyo)*, 120, 66–73.

Selective Precipitation of Salts on the Surface of a Gel State Phosphatidylcholine Membrane

Kazutoshi Iijima, Teruhiko Matsubara, and Toshinori Sato*
Department of Biosciences and Informatics, Keio University, 3-14-1 Hiyoshi, Kouhoku-ku, Yokohama 223-8522

(Received April 3, 2007; CL-070358; E-mail: sato@bio.keio.ac.jp)

We identified precipitates of salts on phospholipid bilayers in solution with an atomic force microscope and X-ray fluorescence analyzer. The precipitates on the surface of a dipalmitoyl phosphatidylcholine membrane in a gel state were found in Tris-buffered saline and grew with time. The salts precipitated were considered to be NaCl in buffer.

In physiological conditions, plasma membranes of animal cells are exposed to various ions. The interactions of phospholipid bilayers with monovalent and divalent ions have been investigated using ^{2}H NMR spectroscopy,[1] and the dependency of electrostatic potential on the variety of ion was evaluated according to the Gouy–Chapman theory of a diffuse double layer.[2] Recently, the interaction of sodium chloride (NaCl) with a 1-palmitoyl-2-oleoyl phosphatidylcholine (POPC) and dipalmitoyl phosphatidylcholine (DPPC) bilayer was investigated by using molecular dynamic simulations, and it was revealed that NaCl in solution altered the conformation of phosphatidylcholine head groups and slightly changed the ordering of hydrocarbon tails.[3,4] However, the influence of the state of the phosphatidylcholine membrane on the binding of NaCl has not been investigated.

In the present study, we employed an atomic force microscope (AFM) and an X-ray fluorescence analyzer to observe the precipitation of salt on phospholipid bilayers in solution. The procedures for the preparation of lipid bilayer on mica were shown in Figure 1. An air–water interface lipid monolayer of POPC was prepared on a Langmuir–Blodgett trough (FSD-220, USI System Co., Ltd., Japan) at 25 °C with a subphase of Milli-Q water. The POPC monolayer was transferred to freshly cleaved mica by horizontal deposition at a surface pressure of 35 mN·m^{-1} and dried overnight in a desiccator. A second lipid monolayer of either DPPC or POPC was transferred to the POPC-coated mica by horizontal deposition at a surface pressure of 30 mN·m^{-1}. AFM measurements of the lipid bilayers cumulated on mica were carried out on a SPA-300 (Seiko Instruments Inc., Japan) in Milli-Q water or buffers at 25 °C. A 200-μm-long soft cantilever (SN-AF01, Olympus Optical Co., Ltd.) with integrated pyramidal silicon nitride tips having a spring constant of 0.02 N·m^{-1} was used for all measurements. A typical scan rate was 1 Hz.

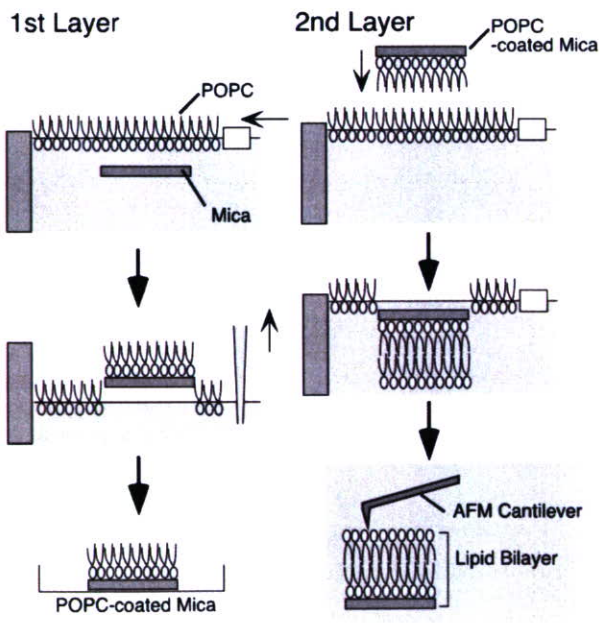

Figure 1. The procedures for the preparation of lipid bilayer on mica.

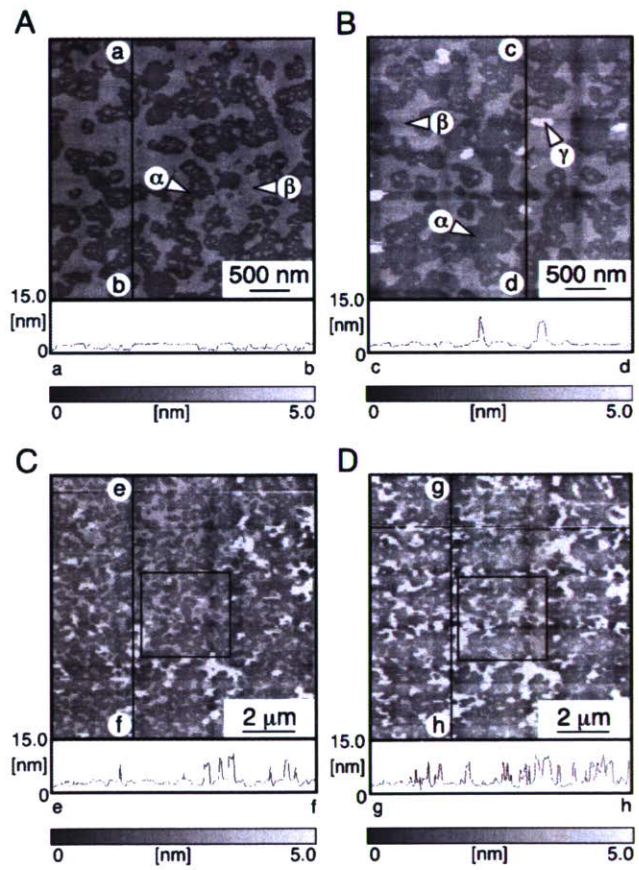

Figure 2. AFM images of the surface of the DPPC membrane in (A) water and (B–D) TBS. Incubation with the TBS lasted (B) 5 min, (C) 10 min, and (D) 20 min. Cross sections are shown at the bottom of each AFM image. Squares in (B) and (C) mean identical areas with (B).

A typical AFM image of the DPPC membrane was shown in Figure 2A. Domains 1.0 nm in height (β) from the lower region (α) were observed. This result suggested that two-phase state having different heights coexisted. The domain β and region α were considered to correspond to DPPC in a gel state and liquid-crystal state, respectively. Brewster angle microscopy showed that at 25 °C, DPPC separated into the two domains, a gel state and a liquid-crystal state.[5] The present AFM results were well consistent with the literature.

Then, the water phase covering the lipid membrane was replaced with Tris-buffered saline (TBS; 50 mM Tris-HCl, 150 mM NaCl, pH 7.5) in the AFM apparatus. After 5 min, a new domain γ having a height of 8–10 nm was observed by AFM (Figure 2B, bright dots). The occupied areas of domain γ were 1.6, 6.2, and 14.9% at 5, 10, and 20 min, respectively. Though the area of γ increased depending on the incubation time, the height showed no increase (Figures 2B, 2C, and 2D). Since domain γ was not observed in Tris-HCl buffer (50 mM Tris-HCl, pH 7.5), the precipitates were considered to be NaCl. Interestingly, domain γ was detected only on domain β corresponding to DPPC in a gel state (Figures 2B, 2C, and 2D). The precipitates disappeared on washing with Milli-Q water (data not shown). On DPPC membranes incubated with Tris-HCl buffer containing other salt such as KCl and $MgCl_2$, the precipitation was not observed (data not shown).

The atomic species of the precipitates observed on the membrane were identified by energy dispersive X-ray fluorescence (EDXRF) analysis. The lipid membranes cumulated on mica were incubated with TBS, then the solution was removed, and measurements were carried out at 25 °C with an X-ray analytical microscope (XGT-2700, Horiba, Ltd.). It was difficult to detect the spectrum from sodium because the energy of the spectrum is as low as the detection limit of the instrument. Existence of chlorine was estimated from Kα and Kβ peaks in EDXRF spectrum at an operating voltage of 15 kV with a standard less quantification procedure.[6] The EDXRF of each sample was done with a 30-s counting time. When the DPPC membrane was exposed to TBS for a couple of seconds, the chlorine peaks of Kα and Kβ from chlorine were slightly detected (intensity of chlorine, 0.35 ± 0.31 cps·mA^{-1}, Table 1). After 45 min, these peaks were clearly detected (2.07 ± 0.36 cps·mA^{-1}). When the DPPC membrane was exposed to Milli-Q water, chlorine was not detected. Increasing of the intensity of chlorine depending on the incubation time was observed. The existence of chlorine strongly supported that the precipitates on the DPPC monolayer corresponded to NaCl.

The formation of precipitates of NaCl only on solid DPPC may relate to the ordering of electric dipoles of zwitterionic phosphatidylcholine (PC). A molecular dynamics simulation has shown that Na^+ ions were closer to phosphate groups and Cl^- has some coordination with nitrogen in choline.[4] The interactions of Na^+ and Cl^- with PC would be due to the crystallization of NaCl on PC membrane.

To examine the influence of the kind of ion and pH of the buffer on the precipitation of salt, AFM measurements were performed using a phosphate-buffered saline (PBS). The precipitation of NaCl on DPPC was observed in PBS at pH 7.2, but not at pH 5.7 (data not shown). A quaternary amino group is fully positive at any reasonable pH value, and an ionizable phosphate group has an intrinsic pK of $\approx$1.5.[7] Although phosphatidylcholine is in a zwitterionic state at both pH 7.2 and 5.7, the protonation of the phosphate groups increases at pH 5.7.

Table 1. Intensities of chlorine on DPPC membrane surface by X-ray fluorescence analyses

Condition	Intensity of Chlorine /cps·mA^{-1}
Milli-Q	0.05 ± 0.07
PBS (few seconds)	0.35 ± 0.31
PBS (45 min)	2.07 ± 0.36

Next, POPC or mixed DPPC/cholesterol (60:40 by mol.) membranes were employed to examine the influence of membrane fluidity on the precipitation of salts. For the POPC membrane in a liquid-crystalline state, no precipitation was observed with the AFM, and X-ray fluorescence analysis showed no signal from chlorine (data not shown). Furthermore, for the DPPC/cholesterol (60:40) membrane, precipitation was not observed. Using differential scanning calorimetry, it has been found that cholesterol decreases the crystallinity of phospholipids in a gel state.[8] These results suggested that the ordered electric dipoles of the PC head group induced the precipitation of salts on DPPC membrane.

In conclusion, we observed the selective precipitation of salts on a gel state DPPC membrane. AFM observations of lipid membranes in solution brought the unexpected precipitation of salts on the surface of the DPPC membrane. The precipitated salts were considered to be NaCl from the composition of the buffer and results of X-ray fluorescence analysis. Further investigation will improve understanding of the interaction of inorganic ions with biomembranes and the preparation of organic–inorganic hybrid materials.

References

1 P. M. Macdonald, J. Seelig, *Biochemistry* **1988**, *27*, 6769.
2 M. Eisenberg, T. Gresalfi, T. Riccio, S. McLaughlin, *Biochemistry* **1979**, *18*, 5213.
3 J. N. Sachs, H. Nanda, H. I. Petrache, T. B. Woolf, *Biophys. J.* **2004**, *86*, 3772.
4 S. A. Pandit, D. Bostick, M. L. Berkowitz, *Biophys. J.* **2003**, *84*, 3743.
5 W. R. Schief, L. Touryan, S. B. Hall, V. Vogel, *J. Phys. Chem. B* **2000**, *104*, 7388.
6 a) J. Blanc, S. Populaire, L. Perring, *Anal. Sci.* **2005**, *21*, 795. b) H. Kanada, Y. Ishikawa, T. Uomoto, Abstracts of papers, 6th International Symposium Non-Destructive Testing in Civil Engineering, St. Louis, MO, U.S.A., August 14–18, **2006**.
7 a) J. F. Tocanne, J. Teissie, *Biochim. Biophys. Acta* **1990**, *1031*, 111. b) S. Furuike, V. G. Levadny, S. J. Li, M. Yamazaki, *Biophys. J.* **1999**, *77*, 2015.
8 R. A. Haberkorn, R. G. Griffin, M. D. Meadows, E. Oldfield, *J. Am. Chem. Soc.* **1977**, *99*, 7353.

Published on the web (Advance View) June 9, 2007; doi:10.1246/cl.2007.860

Available online at www.sciencedirect.com
ScienceDirect
Carbohydrate Research 342 (2007) 1895–1903
Carbohydrate RESEARCH

Structural transition of a 15 amino acid residue peptide induced by GM1

Naoki Fujitani,[a] Hiroki Shimizu,[b,*] Teruhiko Matsubara,[c] Takashi Ohta,[b] Yuuki Komata,[a] Nobuaki Miura,[a] Toshinori Sato[c] and Shin-Ichiro Nishimura[a,b,*]

[a]*Division of Advanced Chemical Biology, Graduate School of Advanced Life Science, Frontier Research Center for Post-Genomic Science and Technology, Hokkaido University, Sapporo 011-0021, Japan*
[b]*Drug-Seeds Discovery Research Laboratory, Hokkaido Center, National Institute of Advanced Industrial Science and Technology (AIST), Sapporo 062-8517, Japan*
[c]*Department of Biosciences and Informatics, Keio University, Yokohama 223-8522, Japan*

Received 16 February 2007; received in revised form 11 May 2007; accepted 15 May 2007
Available online 2 June 2007

Abstract—The ganglioside GM1-binding peptide, p3, with a sequence of VWRLLAPPFSNRLLP, displayed a clear structural alteration depending on the presence or absence of GM1 micelles. The three-dimensional structures of the p3 peptide in the free and GM1 bound states were analyzed using two-dimensional NMR spectroscopic experiments with distance-restrained simulated annealing calculations. The NMR experiments for the p3 peptide alone indicated that the peptide has two conformers derived from the exchange of cis and trans forms at Pro^7–Pro^8. Further study with theoretical modeling revealed that the p3 peptide has a curb conformation without regular secondary structure. On the other hand, the NMR studies for the p3 peptide with the GM1 micelles elucidated a trans conformer and gave a structure stabilized by hydrophobic interactions of β- and helical turns. Based on these structural investigations, tryptophan, a core residue of the hydrophobic cluster, might be an essential residue for the recognition of the GM1 saccharides. The dynamic transition of the p3 peptide may play an important role in the function of GM1 as a multiple receptor as in the traditional pathway of the infection by cholera toxin.

Keywords: Molecular induction; Molecular recognition; GM1; Functional peptide; p3 Peptide

1. Introduction

With the recent success of the human genome analysis, in the life-science research field it is natural to become focused not only on protein structure but also on protein structure–function relationships. Nuclear magnetic resonance spectroscopy is a powerful tool for the study of molecular structures and allows for the analysis of the solution phase structure once the target compound has been dissolved in a suitable deuterated solvent. Unfortunately, the usual target proteins are often too big to study by NMR, which is best for the analysis of proteins smaller than 15 kDa and a maximum of 30 kDa.[1] Although the Kay[2] and Wüthrich[3] groups have reported NMR studies for larger proteins, 723 residues and 900 kDa, respectively, neither was a complete determination. To overcome this problem, designing partially mimetic proteins or the use of part of the protein as the NMR research target has been widely explored, but in many cases the original function is lost due to changes in overall conformation or entropy penalties.

Based on these difficulties, we planned an 'opposite' approach to study protein function, which focuses on 'functional small-module peptides'. We can then study conformational or dynamics details by NMR more easily because the molecular size is small enough for NMR spectroscopy. After elucidation of the binding details, a

* Corresponding authors. Tel.: +81 11 857 8497; fax: +81 11 857 8435 (H.S.); tel.: +81 11 857 8472; fax: +81 11 857 8441 (S.-I.N.); e-mail addresses: hiroki.shimizu@aist.go.jp; shin@glyco.sci.hokudai.ac.jp; tiger.nishimura@aist.go.jp

0008-6215/$ - see front matter © 2007 Elsevier Ltd. All rights reserved.
doi:10.1016/j.carres.2007.05.026

search for identical or similar linear or three-dimensional structures in the Protein Data Bank is carried out. The hit protein will have the same or similar function as the original peptide. Even if we cannot find any similar proteins in the Protein Data Bank, we can design efficiently, based on this knowledge, functional proteins, or so called 'artificial enzymes'.

Gangliosides are neuraminic acid-bearing glycosphingolipids found in eukaryotic cells and are the major sialylated glycoconjugates in the brain.[4] Through their carbohydrate moieties, they are receptors for viral and bacterial toxins, contribute to cell–cell and cell–matrix interactions and regulate cell growth.[5–8] Therefore, it is expected that the elucidation of the mechanism and inhibition of ganglioside–toxin interactions will potentially prevent various diseases.

In a previous study,[9] we presented three types of novel peptides that bind to the pentasaccharide portion of GM1 (β-D-Gal*p*-(1→3)-β-D-Gal*p*NAc-(1→4)(α-D-Neu*p*Ac-(2→3))-β-D-Gal*p*-(1→4)-β-D-Glc*p*-(1→1′)-Cer), which were identified with the improved phage display technique. One, called 'p3', strongly binds to GM1 saccharides with a 1.2 μM dissociation constant by QCM (quartz crystal microbalance).[10] This is the first reported artificial peptide with no homology to any native proteins and peptides with the ability to recognize GM1. The p3 peptide is expected to be an efficient substance for the development of GM1-binding inhibitors as well as an optimal model for clarifying ganglioside–peptide interactions. In this study, using p3, which has the primary sequence VWRLLAPPFSNRLLP, we studied the interaction of the peptide with GM1 oligosaccharide using NMR methods and computational methods.

2. Results

2.1. NMR analysis of the p3 peptide

Well-resolved spectra of p3 were obtained for both conditions (with or without ganglioside GM1) as described in Section 4 and the observed cross-peaks were assigned completely according to the sequence specific assignment of Wüthrich.[11] The identification of spin systems of the amino acids was based on scalar coupling patterns observed in TOCSY experiments, and complemented with ROESY and NOESY measurements. The sequential connectivities were identified by the assignments of distance information, ROEs or NOEs, which are $^{\alpha}$H(i)–NH($i+1$) ($d_{\alpha N}$), $^{\beta}$H(i)–NH($i+1$) ($d_{\beta N}$), and NH(i)-NH($i+1$) (d_{NN}). A summary of the sequential assignments is shown in Figure 1.

In the case of the spectra with p3 alone, it was found that each residue showed two kinds of scalar coupling networks in the TOCSY spectra at the beginning of spectral analyses (Fig. 2). One had strong intensity and

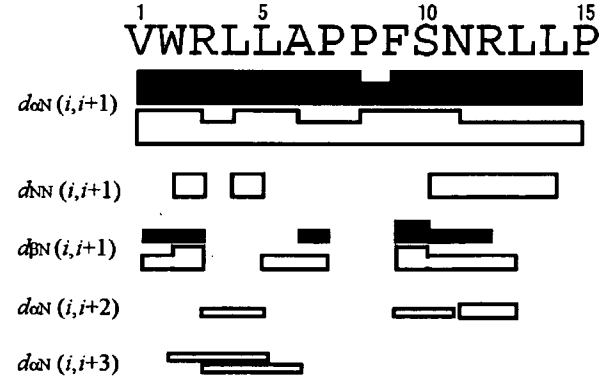

Figure 1. Summary of ROE or NOE connectivities of p3 in the presence and absence of GM1 oligosaccharide. The sequential ROEs and NOEs, $d_{\alpha N}(i,i+1)$, $d_{\beta N}(i,i+1)$ and $d_{NN}(i,i+1)$, and the medium-range NOEs, $d_{\alpha N}(i,i+2)$ and $d_{\alpha N}(i,i+3)$, are represented by bars and classified into strong, medium, weak, and very weak intensities according to the height of the bars. Black bars indicate the ROE connectivities of the peptide in the free state, and white bars represent complex states with GM1 micelles.

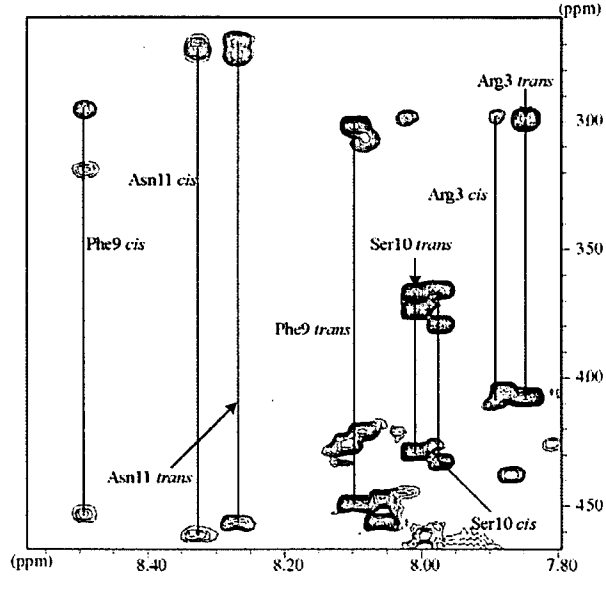

Figure 2. NH-aliphatic region of TOCSY spectrum of the free state of p3. Two different spin systems were detected for each residue. The assignments of Arg[3], Phe[9], Ser[10], and Asn[11] are labeled in this figure. This TOCSY spectrum was recorded with 80 ms of the spin-lock time.

the other was weak, which suggested slow conformational exchange of the protein that occurred in aqueous solution. ROE analyses successfully revealed the details of the coupling networks observed in the TOCSY spectra. In the one with weak intensity, the Pro[7]–Pro[8] peptide bond was determined to have cis conformation because the detection of ROE $d_{\alpha\alpha}$ was of stronger intensity than that of $d_{\alpha\delta}$. Another network with strong intensity had a trans conformation in this site. In this solution sample, 114 ROEs for the trans conformer were gathered as distance information for structural calculation although sufficient inter-residual ROEs were not

observed for the *cis* peptide. In this study, we defined a *trans* peptide as a major component of the p3 peptide. As the most impressive information reflecting the structure of this peptide, two long-range ROE between Trp^2εH3 and Leu^{14}βHs, and between Trp^2εH3 and Leu^{14}γH were observed, which suggested that the N- and the C-terminal of the peptide were in close proximity. Whereas the ROEs between hydrophobic side chains (i to $i+1$, i to $i+2$ relations) were observed, other characteristic ROEs for secondary and tertiary structure were not observed. Unfortunately only poor NOESY spectra were obtained, because $\omega\tau_c$ (τ_c: molecular correlation time) of the peptide might become zero depending on the intensity of NOE. Thus, ROESY experiments were used to obtain the proton–proton distance information.

To reveal the structure of this GM1-binding peptide, NMR experiments were carried out with the p3-GM1 complex (p3 peptide 3 mM with GM1 0.3 mM). Because the primary critical micellar concentration of GM1 is 3.32 μM,[12] GM1 under these conditions would form a micelle. The fact that the p3 was found by the QCM method to a GM1 monolayer indicated that the peptide surely interacts with a pentasaccharide region of GM1.[10] Thus, forming a micelle of GM1 was not an improper condition. Moreover, it could be an advantage to avoid nonspecific binding with the ceramide portion of the molecule.

In TOCSY spectra, three kinds of scalar coupling networks were observed, which were derived from the GM1-binding state and the free state of trans and cis conformers. The NOESY experiments gave sufficient signals derived from the complex, though the signals of the free state of p3 were found only with very weak intensity such as NOESY spectra. A total of 146 NOEs could be assigned from complex state NOESY spectra for constraints of structure calculation. As one of the characteristic NOEs, six sequential NOEs between backbone amides, Trp^2–Arg^3, Leu^4–Leu^5, Ser^{10}–Asn^{11}, Asn^{11}–Arg^{12}, Arg^{12}–Leu^{13}, and Leu^{13}–Leu^{14}, were found, whereas no NH–NH NOEs were observed in the spectra of p3 alone (Fig. 3). A total of 28 and 12 new sequential and medium-range NOEs, respectively, were also discovered suggesting that the peptide forms a stable conformation. Furthermore, NOEs derived from the aromatic ring of Trp^2, including long-range interactions, were newly identified (Fig. 4), indicating restriction of Trp^2 mobility in the presence of GM1.

For the samples of p3 alone and the p3–GM1 complex, the $^3J_{HN\alpha}$ were determined by high-resolution DQF–COSY spectra to estimate the restraint of dihedral angle ϕ. In the free state, $^3J_{HN\alpha}$ of Arg^3 was more than 8.0 Hz (dihedral angle ϕ is approximately −120°), and Leu^5 and Leu^{14} were less than 6.0 Hz (dihedral angle ϕ is approximately −60°). On the other hand, $^3J_{HN\alpha}$ of Trp^2, Leu^5, Ala^6, and Phe^9 were greater than 8.0 Hz, and Arg^3, Asn^{11} and Leu^{12} were less than 6.0 Hz. These results indicate that the conformation of the peptide was changed by the addition of GM1. In particular, Arg^3, Leu^5 and Ala^6 represented a drastically changed dihedral angle ϕ, and the C-terminal region including Asn^{11} and Arg^{12} was predicted by constructing a helical conformation by the combination of dihedral angles and NH–NH NOEs.

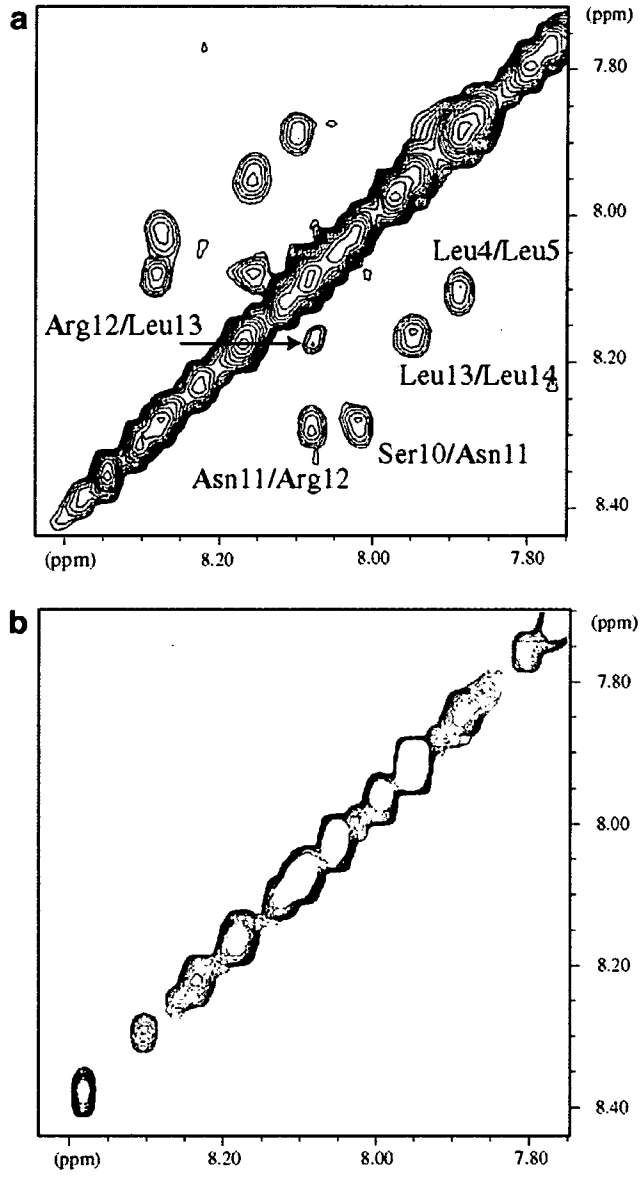

Figure 3. NH–NH region of ROESY and NOESY spectra of p3 in the presence (a) and absence (b) of GM1 oligosaccharide. Sequential NOEs between backbone amides were detected in the complex state with p3 (a), although corresponding ROEs could not be observed in the case of p3 alone (b). Four of six NOEs are shown in (a) with assignment labels. These ROESY and NOESY spectra were performed with 250 ms of mixing time.

2.2. Structure determination by NMR

We carried out the structural calculations with the program CNS 1.1[13] to determine the three-dimensional

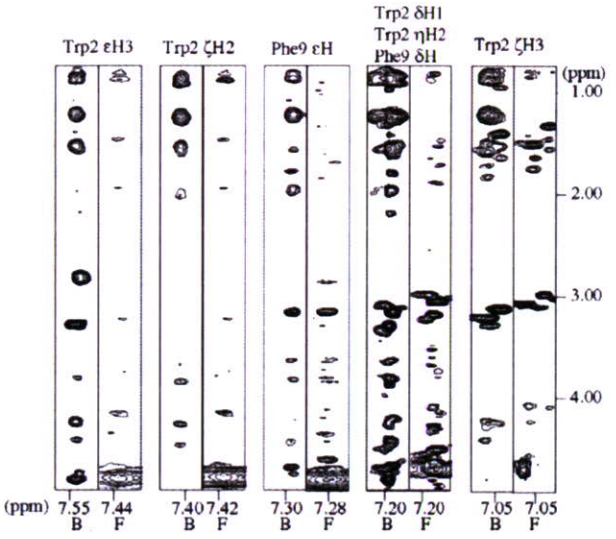

Figure 4. Aromatic–aliphatic regions of ROESY spectra of the p3 alone and NOESY spectra of the p3 with GM1 oligosaccharide. The stripped spectra of the region of aromatic protons are shown to investigate the increment of NOEs led by the addition of GM1. On the top of each strip, the name of the observed aromatic proton and characters B and F in the figure indicate the bound and the free states of p3, respectively.

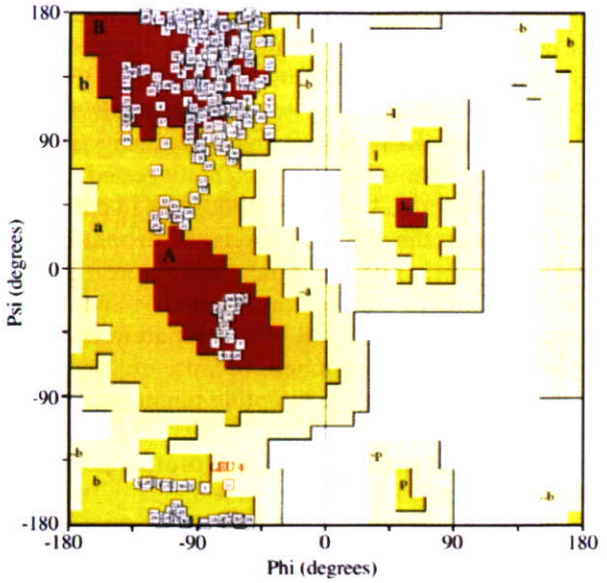

Figure 5. Ramachandran plot of the obtained 30 structures of p3. All residues except for prolines are located on the allowed region, suggesting that p3 has a general structure without irregular conformation.

solution structure of the p3 GM1-binding peptide, in the presence and absence of the GM1 micelle. Calculations were carried out using the 114 and 146 intramolecular ROEs and NOEs as distance constraints in the absence or presence of GM1, respectively. The 114 distance restraints included 66 intraresidue ($|i-j|=0$), 29 sequential ($|i-j|=1$), 17 medium ($2\leqslant|i-j|\leqslant 4$), and two long-range ($|i-j|\geqslant 5$) ROEs, and the 146 distance constraints included 57 intraresidue ($|i-j|=0$), 57 sequential ($|i-j|=1$), 27 medium ($2\leqslant|i-j|\leqslant 4$), and five long-range ($|i-j|\geqslant 5$) NOEs. In the first step, the structure calculations were performed without the restraints of dihedral angles, but with only the distance constraints estimated from NOE intensities. Restraints with large violations were removed or modified in this step. In the next step, a total of three and seven dihedral angle ϕ restraints were added for calculation of the p3 peptide alone and the p3–GM1 complex cases, respectively. In the final step, to locate each dihedral angle ϕ on the allowed position in the Ramachandran plot, highly loose constraints $-100\pm 80°$ were applied.

Finally, a family of 25 accepted three-dimensional structures were selected with the lowest potential energies that contained no experimental violations greater than 1.0 Å and 1° in the distance and torsion angle restraints, respectively. In the Ramachandran plots shown in Figure 5, 99.7% and 99.3% for the p3 peptide alone and the p3–GM1 complex, respectively, of the backbone dihedral angles of the 25 converged structures fell within the allowed regions. A summary of the energetic statistics for the GM1-binding peptide is shown in Table 1.

Table 1. Structural statistics for p3 in the presence or absence of GM1 micelles

	Absence of GM1	Presence of GM1
Average potential energies (kcal mol^{-1})[a]		
E_{total}	22.81 ± 1.71	32.29 ± 2.88
E_{bonds}	0.46 ± 0.07	1.04 ± 0.18
E_{angle}	14.95 ± 0.23	18.66 ± 1.36
E_{impr}	0.32 ± 0.09	1.14 ± 0.23
E_{VDW}[b]	5.16 ± 1.17	9.78 ± 1.40
E_{NOE}[b]	1.92 ± 0.53	1.90 ± 0.94
E_{cdih}[b]	0.009 ± 0.001	0.11 ± 0.05
RMSD from idealized geometry		
Bonds (Å)	0.0013 ± 0.0001	0.0020 ± 0.0002
Angles (°)	0.4461 ± 0.0035	0.4981 ± 0.0180
Impropers (°)	0.1182 ± 0.0015	0.2250 ± 0.0022
Pairwise RMSD of 25 structures from Val^{1} to Leu^{14} (Å)		
Backbone atoms (N, Cα, C′)	1.31 ± 0.36	0.37 ± 0.11
All heavy atoms	2.52 ± 0.67	1.14 ± 0.21

All energies and RMSD values were calculated using the CNS 1.1[28] and MOLMOL[31] programs, respectively.

[a] E_{impr}, E_{VDW}, E_{NOE}, and E_{cdih} are the energy of improper torsion angles, the van der Waals repulsion energy, the square-well NOE potential energy and the dihedral potential energy, respectively.

[b] The force constants for the calculations of E_{VDW}, E_{NOE}, and E_{cdih} were 4.0 kcal mol^{-1} Å^{-4}, 50 kcal mol^{-1} Å^{-1} and 200 kcal mol^{-1} rad^{-2}, respectively.

Figure 6 shows the structures of p3 in the presence and absence of GM1 oligosaccharide. For the p3 without GM1, the pairwise RMSD values for the 25 lowest-energy structures were found to be 1.31 ± 0.36 Å for backbone atoms and 2.52 ± 0.67 Å for all heavy

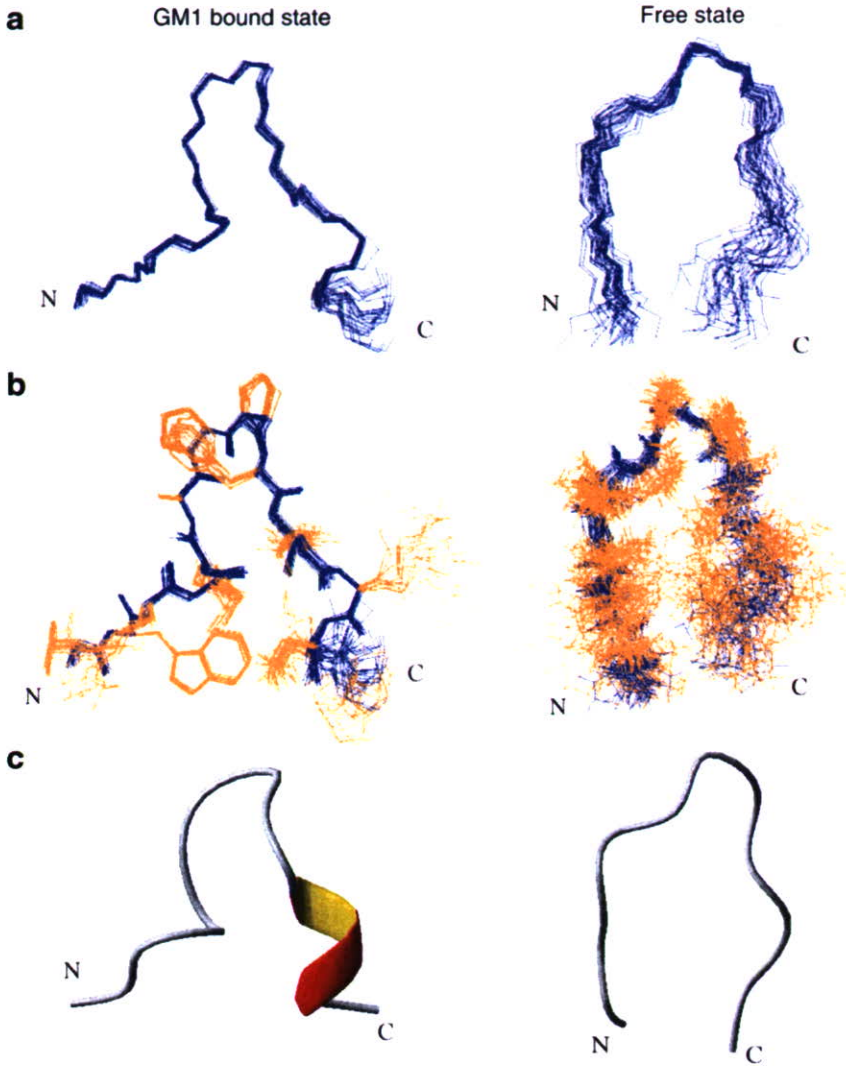

Figure 6. Three-dimensional structures of p3. Twenty five structures are superimposed to the backbone atoms from Val^{1} to Leu^{14}. The structures of p3 in the presence and absence of GM1 micelles are displayed in the left and right columns, respectively. (a) and (b) represent structures of the backbone atoms and all heavy atoms including side chains, respectively. Blue and orange lines indicate the backbone and side chains, respectively. (c) is the lowest-energy models of 25 structures. This figure was generated by MOLMOL[33] software.

atoms when the structures were fit in the region of Val^{1}–Leu^{14}. From the NMR data, p3 without GM1 formed a curb at the middle and had variable conformation without regular secondary structure. This peptide, however, had the specific conformations in local areas, for example, Val^{1}–Ala^{6} and Pro^{7}–Arg^{12}, with 0.46 ± 0.15 and 0.58 ± 0.18 Å of the RMSD value of backbone atoms, respectively. Hydrophobic interactions stabilized the conformations of both regions. The region from Val^{1} to Ala^{6} had a hydrophobic surface constructed to the side chains of Trp^{2}, Leu^{4}, and Leu^{5} and the region from Pro^{7} to Arg^{12} formed a rigid turn with the hydrophobic contacts of proline rings and the aromatic ring of Phe^{9}.

On the other hand, the greatly converged structure of the peptide in the presence of GM1 micelle was determined to have RMSD values of 0.37 ± 0.11 and 1.14 ± 0.21 Å for the backbone atoms and all heavy atoms, respectively. The fluctuation of the peptide was reduced significantly compared to the peptide alone. The 25 lowest-energy structures in the region of Val^{1}–Leu^{14} are superimposed in Figure 6. The molecule maintained the bent structure with the rigid turn made by the Pro^{7}–Pro^{8} portion. The most noteworthy feature of this structure is the hydrophobic cluster, including Trp^{2}, Leu^{4}, Leu^{5}, Leu^{13}, and Leu^{14}. The residues forming a hydrophobic surface, Trp^{2}, Leu^{4}, and Leu^{5} in the case of the structure absent from GM1, are toward the inside of the peptide, and the aromatic ring of Trp^{2} is surrounded by the N- and C-terminal leucines. Moreover, two stable turns were found in the regions of Trp^{2}–Leu^{5} and Ser^{10}–Arg^{12}. The former was identified as a β-turn using the standard criterion with the distance between $^{\alpha}C(i)$ and $^{\alpha}C(i+3)$ as less than 7 Å.[13] The average distance between $^{\alpha}C$ atoms of Trp^{2} and Leu^{5}

was 5.35 Å. This turn had a nearly type I β-turn conformation from the viewpoint of the dihedral angles of constructing residues. However, no NMR information about the hydrogen bonding was obtained, and furthermore it was clarified that there was no intra-turn hydrogen bond in the calculated structures. This turn was therefore defined as a $\beta_E\gamma$-type turn,[14] that is, a type-IV β-turn (miscellaneous type) according to the classical nomenclature. The second turn was a helical turn like the conformation of the 3_{10} helix. The C-terminal region of p3 showed a highly disordered structure absent from GM1, therefore this region might play an important role in binding to GM1 saccharides.

2.3. Molecular dynamics study for the p3

Molecular dynamics (MD) simulations were also carried out. Two major structures were obtained with the MD calculations within 40 ns at 325 K, preceded by the MD to generate the starting geometries at high temperature. These were in good agreement with the fluctuating conformations obtained by NMR experiments. One of these had a curb form at the middle of p^3, Pro^7–Phe^9, and there were no characteristic hydrogen bonds in half of the N-terminus, which meant that the peptide did not have a specific secondary structure (Fig. 7). Although the RMSD between the structures from the NMR study and the MD simulation was large (4.67 Å), both structures had the same topology. This suggested that the MD simulations were able to support the NMR experiments. Figure 8 shows the other structure obtained by MD with the bound p3 NMR backbone structure. Although we have not considered the existence of GM1 during these simulations, we found that the RMSD for the backbone structure of 3.56 Å was smaller than the case in Figure 8.

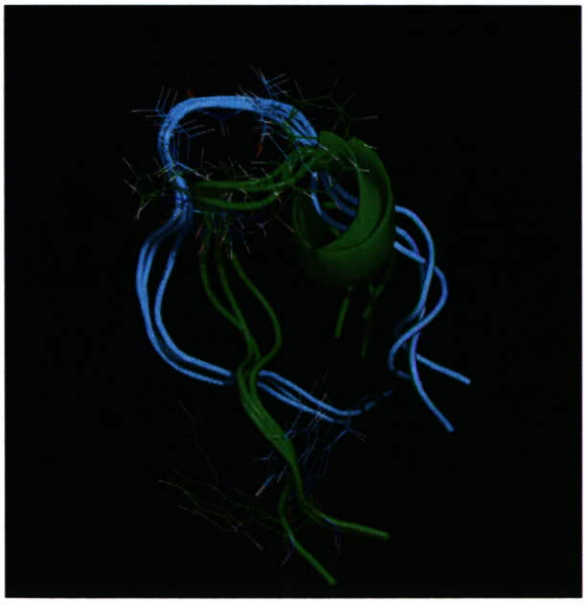

Figure 7. Superimposed structure of p3 from MD simulations (green) and from NMR data without GM1. Both have the same topologies including (i) curb structure at the middle and (ii) no secondary structure although MD simulation showed 'helix-like' predicted structure at the C-terminal area. Side chains of key residues that bind GM1, Pro^7–Phe^9 and Trp^2, are also shown.

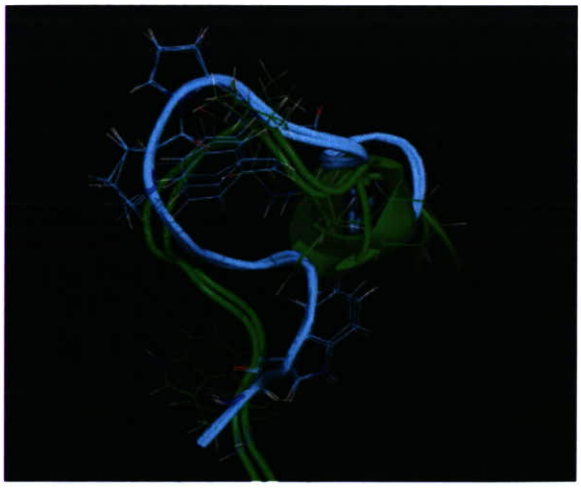

Figure 8. Superimposed structure of p3 from MD simulations (green) and from NMR data with GM1. Although the MD calculations were performed without any ligand, the structure from MD was similar to the structure from NMR with GM1. Side chains of key residues that bind GM1, Pro^7–Phe^9 and Trp^2, are also shown.

3. Discussion

In summary, the structure of the p3 peptide was stabilized completely in the presence of the GM1 oligosaccharide, which existed in the micelle form. In the bound form, the peptide is stabilized by forming stable β- and helical turns, whereas the Pro^7–Pro^8 region contributing to the bend in the peptide structure was preserved.[15,16] Therefore, it can be suggested that the N- and the C-terminal regions underwent drastic conformational change upon the binding of the GM1 pentasaccharide (Fig. 6). Unfortunately, no characteristic intermolecular NOEs that could suggest a specific binding site were observed in this study because GM1 formed micelles in aqueous solution and thus gave significant line-broadening in the NMR spectra.

Previous studies on lectins proposed that the modular structure of the aromatic ring of tryptophan on the β-turn, known as the carbohydrate-binding module (CBM), plays a key role in the hydrophobic interaction with the nonpolar face of monosaccharide rings.[17–19] Based on the structural analyses of p3, Trp^2 of the bound state was also included in the β-turn and constructed a hydrophobic core. We, therefore, propose that Trp^2 would be an essential residue for binding to

GM1 pentasaccharide. Moreover, for the representative example of the recognition of NeuAc, arginine binds to the carboxyl group of NeuAc through the electrostatic interaction in the coat protein of murine polyoma virus.[20] This GM1-binding peptide had two arginines, Arg^3 and Arg^{12}, located on the β-turn and the helical turn, respectively. From the viewpoint of the solution structure of the bound state, the side chain of Arg^{12} was exposed to solvent with more disordered direction than that of Arg^3, which would suggest that Arg^3 is strongly involved in the recognition of NeuAc in GM1.

Although Honda et al. reported the conformation of a 10 amino acid residual peptide,[21] it is difficult, in general, for a small peptide to form a steady conformation and create a stable binding site for oligosaccharides in aqueous solution. Thus our results indicate that the structure of ligand peptide was controlled by the carbohydrate platform. Whereas it is frequently reported that gangliosides on the cell surface behave as receptors to various ligands, we believe that the regulation of the protein and peptide structure is also one of the most essential functions of carbohydrates. As another interesting study on ganglioside–peptide interaction, it has also been reported that enkephalins, endogenous neurotransmitters consisting of five amino acids have altered folding in the bound state with GM1 micelle.[22] This study indicated that enkephalins had an induced rigid turn structure by interaction with the GM1 micelle, which was very similar with the structure in bicelles.[23] Moreover, the nonapeptide bradykinin, a neuropeptide with an antiphlogistic effect, was also recently confirmed to undergo conformational change on binding to GM1 micelles.[24] These drastic transitions of the structure of ligand peptide on GM1 surface are likely to play an important role in the ignition of sequential events like the traditional pathway of cholera toxin infection.

4. Experimental

4.1. General

Unless otherwise stated, all commercially available solvents and reagents were used without further purification. Fmoc amino acid derivatives and resin were purchased from NOVA Biochem Co. Ltd. Automatic peptide synthesis was performed with Advanced Chem Tech MODEL Apex396 peptide synthesizer. HPLC was performed on a Hitachi HPLC system equipped with an L-7150 intelligent pump, an L-7420 UV detector and reversed-phase C18 column, Inertsil® ODS-3 (20 × 250 mm) at a flow rate of 5.0 mL min^{-1}. The eluate was monitored by UV absorption at 220 nm. MALDI-TOF MS analyses were performed with the Bruker REFLEXIII mass spectrometry with 2,5-dihydroxybenzoic acid (DHB).

4.2. Preparation of samples

GM1 was purchased from Wako Pure Chemical Industries, Ltd. (Osaka, Japan) and was used without further purification.

The p3 peptide, VWRLLAPPFSNRLLP,[9,10] was synthesized on Fmoc-Pro-OH preloaded 2-chlorotrityl chloride resin (0.66 mmol/g) using an automatic peptide synthesizer (a common solid-phase peptide synthetic method with Fmoc strategy) in four batches on 0.02 mmol scale each (four portions of 30 mg of preloaded resin each). Fmoc amino acid derivatives, Fmoc-Pro-OH, Fmoc-Leu-OH, Fmoc-Arg(Pbf)-OH, Fmoc-Asn(Trt)-OH, Fmoc-Ser(*t*Bu)-OH, Fmoc-Phe-OH, Fmoc-Ala-OH, Fmoc-Trp(Boc)-OH and Fmoc-Val-OH, were employed. A cycle of automated peptide synthesizer for a 0.02 mmol scale was defined as follows. The resin was treated with 1.5 mL of 20% (v/v) piperidine in DMF and the mixture was stirred for 5 min at ambient temperature. After filtration, the same process was performed but stirred for 15 min. Then, the resin was washed with NMP (*N*-methylpyrrolidine, 1.5 mL) and DMF (1.5 mL). To a mixture of a solution of Fmoc amino acid (4 equiv) and HOBt (*N*-hydroxybenzotriazole, 3.5 equiv) in NMP (600 μL) and a solution of HBTU (2-(1*H*-benzotriazole-1-yl)-1,1,3,3-tetramethyluronium hexafluorophosphate, 4 equiv) and DIEA (diisopropylethylamine, 6 equiv) in DMF (600 μL) was added the resin, and the reaction mixture was stirred for 40 min at ambient temperature. This coupling process was performed twice. After washing the resin with NMP (1.5 mL) and DMF (1.5 mL), nonreactive amino groups were acetyl-capped with 1.5 mL of a mixed solution of Ac_2O (4.75% as v/v) and HOBt (13 mM) in NMP. After completing the peptide synthesis process, the resin was washed with NMP (1.5 mL) and CH_2Cl_2 (1.5 mL), and dried in vacuo. The protected peptide on the resin was treated with 10 mL of a mixed solution of TFA/H_2O/ethanedithiol/triisopropylsilane (94.5/2.5/2.5/1.0 (v/v/v/v)) for 3 h at ambient temperature followed by washing with TFA (2 mL) to remove the peptide from resin and for deprotection of protecting groups such as -*t*Bu, -Trt, -Pbf, and -Boc. The combined solvent was dried with blowing N_2 gas and precipitated from cold dry *tert*-butylmethyl ether. The obtained white solid was purified by HPLC [eluate: solvent A (0.1% TFA in H_2O) and solvent B (0.1% TFA in acetonitrile), gradient; increase from 2% to 60% of B over 60 min]. The fractions containing the desired peptide were collected and lyophilized. The p3 peptide was obtained as a white powder (72 mg, 50% overall yield). Typical NMR data are shown in the figures. Amino acid analysis (theoretical ratio): Asp (Asn) 1.0 (1), Ser 0.8 (1), Ala 1.0 (1), Val 0.9 (1), Leu 4.0 (4), Phe 1.0 (1), Trp 0.9 (1), Arg 2.1 (2); MALDI-TOF-MS calcd for $[M+H]^+$ 1779.043, found $[M+H]^+$ 1779.827.

4.3. NMR measurements

Sample solutions for NMR measurements were prepared by dissolving p3 in a mixed solvent of 10% D_2O, 90% H_2O or 99.9% D_2O, and the sample pH was adjusted to 4.1. All NMR spectra were measured on a Bruker Avance 600 spectrometer equipped with a cryoprobe system operating at 600.13 MHz for the proton frequency. The sample was not spun and the spectra were recorded at a temperature of 300 K. Data acquisition was performed with XWINNMR 3.1 (Bruker) software operating on a Silicon Graphics O2+ workstation. The water signal was suppressed by low-power irradiation during the relaxation delay time and WATERGATE method with 3-9-19 pulse sequence with *x*, *y*, *z*-triple gradient.[25,26] One-dimensional ^1H NMR experiments were performed with a spectral width of 6009.615 Hz, 32K data points and 8 scans. Two-dimensional DQF–COSY,[27] TOCSY,[28,29] ROESY,[30] and NOESY[31] measurements were recorded in a phase sensitive mode. The TOCSY transfer was achieved with the MLEV-17 pulse sequence with spin-locking times of 60, 80, and 100 ms. ROESY and NOESY spectra were recorded with mixing times of 150 and 250 ms, respectively. Except for DQF–COSY determination of the $^3J_{HN\alpha}$, all two-dimensional measurements were recorded with 2048 × 512 frequency data points and zero-filled to yield 2048 × 2048 data matrices. High-resolution DQF–COSY experiments were measured with 4096 × 512 points and zero-filled to a 8192 × 8192 matrix with a 0.73 Hz point resolution. The number of scans for all spectra was 8. The time domain data in both dimensions were multiplied by a sine bell window function with 90° phase shift prior to Fourier transformation. All NMR spectra were processed by software NMRPIPE,[32] and the signals were assigned with the XEASY[33] program on a Silicon Graphics O2 workstation.

4.4. Structure modeling based on NMR data

Three-dimensional structures of p3 were calculated with CNS 1.1[34] program on a Linux workstation. A total of 114 and 146 distance restraints for p3 and the complex of the p3 and GM1 samples, respectively, were used to calculate the family of structures. Moreover, 12 dihedral angle ϕ restraints were used for both sample calculations. Distance restraints for calculations were estimated from the cross-peak intensities in ROESY or NOESY spectra with a mixing time of 150 ms; the estimated restraints were then classified as strong, medium, weak, and very weak, and assigned upper limits of 2.7, 3.5, 5.0, and 6.0 Å, respectively. Pseudo-atom corrections were used for unresolved NOE cross-peaks, methyl protons as well as nonstereospecifically assigned methylene and aromatic protons. In addition, 0.5 Å was added to the upper limit of the distance constraints of only the involved methyl protons according to the report by Clore et al.[35] The restraints of the dihedral angle ϕ were based on $^3J_{HN\alpha}$ coupling constants measured in high-resolution DQF–COSY. For checking of the restraints violation, the PROCHEK-NMR 3.5.4[36] program was used on a Linux workstation, and superimposition of the obtained structures, calculation of RMSD values, and general analyses of GM1-binding peptide were performed with MOLMOL[37] software.

4.5. Ab initio computational structural analysis with molecular dynamics simulation

A molecular dynamics simulation was performed with the AMBER software package version 8.0, using the third-generation point-charge all-atom force field for proteins, also known as ff03.[38] The solvents were implicitly represented by a generalized Born solvent model[39] with no cutoff. p3 was constructed with an extended feature using SYBYL Version 6.9 (Tripos Association, St. Louis, MO).

To generate a variety of conformations of p3 as a starting geometry, 500 steps of a molecular dynamics calculation at 900 K with 2 fs time steps were performed. For all structures, the temperature was gradually lowered until the RMS of the Cartesian elements of the gradient was <0.4 kcal/mol Å. Six groups of conformations were obtained and applied in additional MD calculations. Using each conformer as the starting structures, the 40 ns MD with Berendsen's algorithm[40] was carried out. The temperature and the pressures were kept at 325 K and 1 atm, respectively. In this simulation, the integration time step was 2.0 fs, and SHAKE[41] was applied to constrain all bonds connecting hydrogen atoms. The trajectories were saved every 5.0 ps. A total of 48,000 snapshots were sampled and two major conformers were obtained by a cluster analysis,[42] which are shown in Figures 7 and 8. AMBER 8.0 and PROCHECK were used to analyze the trajectories, and simulations were performed on HP GS1280, Sun Fire 12K, IBM p690, and a Linux cluster with 12 Pentium IV (2 GHz) CPUs.

Acknowledgments

The authors thank Professor Jesús Jiménz-Barbero, Centro de Investigaciones Biologicas, Madrid, Spain, for providing the opportunity to participate in this special issue of Carbohydrate Research on Glycomimetics, and Dr. Nobuaki Nemoto, JEOL Ltd., Akishima, Japan, for useful discussion.

References

1. Gabius, H.-J.; Siebert, H.-C.; André, S.; Jiménez-Barbero, J.; Rüdiger, H. *ChemBioChem* **2004**, *5*, 740–764.

2. Tugarinov, V.; Muhandiram, R.; Ayed, A.; Kay, L. E. *J. Am. Chem. Soc.* **2002**, *124*, 10025–10035.
3. Fiaux, J.; Bertelsen, E. B.; Horwich, A. L.; Wüthrich, K. *Nature* **2002**, *418*, 207–211.
4. Vyas, A. A.; Schnaar, R. L. *Biochimie* **2001**, *83*, 677–682.
5. Lloyd, K. O.; Furukawa, K. *Glycoconjugate J.* **1998**, *15*, 627–636.
6. Suzuki, Y. *Prog. Lipid Res.* **1994**, *33*, 429–457.
7. Hakomori, S. *Annu. Rev. Biochem.* **1981**, *50*, 733–764.
8. Iwabuchi, K.; Yamamura, S.; Prenetti, A.; Handa, K.; Hakomori, S. *J. Biol. Chem.* **1998**, *273*, 9130–9138.
9. Matsubara, T.; Ishikawa, D.; Taki, T.; Okahata, Y.; Sato, T. *FEBS Lett.* **1999**, *456*, 253–256.
10. Matsubara, T.; Iijima, K.; Nakamura, M.; Taki, T.; Okahata, Y.; Sato, T. *Langmuir* **2007**, *23*, 708–714.
11. Wüthrich, K. *NMR of Proteins and Nucleic Acids*; John Wiley and Sons: New York, 1986.
12. Basu, A.; Glew, R. H. *J. Biol. Chem.* **1985**, *260*, 13067–13073.
13. Lewis, P. N.; Momany, F. A.; Scheraga, H. A. *Biochim. Biophys. Acta* **1973**, *303*, 211–229.
14. Wilmot, C. M.; Thornton, J. M. *Protein Eng.* **1990**, *3*, 479–493.
15. Espinosa, J. F.; Gellman, S. H. *Angew. Chem., Int. Ed.* **2000**, *39*, 2330–2333.
16. Aemissegger, A.; Kräutler, V.; van Gunsteren, W. F.; Hilvert, D. *J. Am. Chem. Soc.* **2005**, *127*, 2929–2936.
17. Tormo, J.; Lamed, R.; Chirino, A. J.; Morag, E.; Bayer, E. A.; Shoham, Y.; Steitz, T. A. *EMBO J.* **1996**, *15*, 5739–5751.
18. Din, N.; Forsythe, I. J.; Burntnick, L. D.; Gilkes, N. R.; Miller, R. C., Jr.; Warren, R. A.; Kilburn, D. G. *Mol. Microbiol.* **1994**, *11*, 747–755.
19. Nagy, T.; Simpson, P. J.; Williamson, M. P.; Hazlewood, G. P.; Gilbert, H. J.; Orosz, T. A. *FEBS Lett.* **1998**, *429*, 312–316.
20. Stehle, T.; Yan, Y.; Benjamin, T. L.; Harrison, S. C. *Nature* **1994**, *369*, 160–163.
21. Honda, S.; Yamasaki, K.; Sawada, Y.; Morii, H. *Structure* **2004**, *12*, 1507–1518.
22. Chatterjee, C.; Mukhopadhyay, C. *Biopolymers* **2003**, *70*, 512–521.
23. Marcotte, I.; Separovic, F.; Auger, M.; Gagné, S. M. *Biophys. J.* **2004**, *86*, 1587–1600.
24. Chatterjee, C.; Mukhopadhyay, C. *Biochem. Biophys. Res. Commun.* **2004**, *315*, 866–871.
25. Piotto, M.; Saudek, V.; Sklenář, V. *J. Biomol. NMR* **1992**, *2*, 661–666.
26. Sklenár, V.; Piotto, M.; Leppik, R.; Saudek, V. *J. Magn. Reson. A* **1993**, *102*, 241–245.
27. Rance, M.; Sørensen, O. W.; Bodenhausen, G.; Wagner, G.; Ernst, R. R.; Wüthrich, K. *Biochem. Biophys. Res. Commun.* **1983**, *117*, 479–485.
28. Braunschweiler, L.; Ernst, R. R. *J. Magn. Reson.* **1983**, *53*, 521–528.
29. Bax, A.; Davis, D. G. *J. Magn. Reson.* **1985**, *65*, 355–360.
30. Bothner-By, A. A.; Stephens, R. L.; Lee, J.-M.; Warren, C. D.; Jeanloz, R. W. *J. Am. Chem. Soc.* **1984**, *106*, 811–813.
31. Jeener, J.; Meier, B. N.; Bachmann, P.; Ernst, R. R. *J. Chem. Phys.* **1979**, *71*, 4546–4553.
32. Delaglio, F.; Grzesiek, S.; Vuister, G.; Zhu, G.; Pfeifer, J.; Bax, A. *J. Biomol. NMR* **1995**, *6*, 277–293.
33. Bartels, C.; Xia, T. H.; Billeter, M.; Güntert, P.; Wüthrich, K. *J. Biomol. NMR* **1995**, *6*, 1–10.
34. Brünger, A. T.; Adams, P. D.; Clore, G. M.; DeLano, W. L.; Gros, P.; Grosse-Kunstleve, R. W.; Jiang, J.-S.; Kuszewski, J.; Nilges, M.; Pannu, N.; Read, R. J.; Rice, L. M.; Simonson, T.; Warren, G. L. *Acta Crystallogr., Sect. D* **1998**, *54*, 905–921.
35. Clore, G. M.; Gronenborn, A. M.; Nilges, M.; Ryan, C. A. *Biochemistry* **1987**, *26*, 8012–8023.
36. Laskowski, R. A.; Rullmann, J. A. C.; MacArthur, M. W.; Kaptein, R.; Thornton, J. M. *J. Biomol. NMR* **1996**, *8*, 477–486.
37. Koradi, R.; Billeter, M.; Wüthrich, K. *J. Mol. Graph.* **1996**, *14*, 51–55.
38. Duan, Y.; Wu, C.; Chowdhury, S.; Lee, M. C.; Xiong, G.; Zhang, W.; Yang, R.; Cieplak, P.; Luo, R.; Lee, T.; Caldwell, J.; Wang, J.; Kollman, P. *J. Comput. Chem.* **2003**, *24*, 1999–2012.
39. Onufriev, A.; Bashford, D.; Case, D. A. *Proteins: Struct. Funct. Bioinf.* **2004**, *55*, 383–394.
40. Berendsen, H. J. C.; Postma, J. P. M.; van Gunsteren, W. F.; DiNola, A.; Haak, J. R. *J. Chem. Phys.* **1984**, *81*, 3684–3690.
41. Ryckaert, J.-P.; Ciccotti, G.; Berendsen, H. J. C. *J. Comput. Phys.* **1977**, *23*, 327–341.
42. Jang, S.; Kim, E.; Shin, S.; Pak, Y. *J. Am. Chem. Soc.* **2003**, *125*, 14841–14846.

In Vitro Gene Delivery by pDNA/Chitosan Complexes Coated with Anionic PEG Derivatives that Have a Sugar Side Chain

Mayu Hashimoto,[1] Yoshiyuki Koyama,[2] and Toshinori Sato*[1]
[1]*Faculty of Science and Technology, Keio University, 3-14-1 Hiyoshi, Kouhoku-ku, Yokohama 223-8522*
[2]*Department of Home Economics, Otsuma Women's University, Chiyoda-ku, Tokyo 102-8357*

(Received December 10, 2007; CL-071368; E-mail: sato@bio.keio.ac.jp)

We developed pDNA/chitosan complexes coated with sugar-modified PEG-A/Cs, which are poly(ethylene glycol) derivatives with a side chain of carboxylic acid and sugar. The cationic pDNA/chitosan complexes were coated with anionic sugar-modified PEG-Cs, and anionic ternary complexes were formed. Coating the pDNA/chitosan complexes with maltose- or lactose-modified PEG-A/C (Mal–PEG-A/C or Lac–PEG-A/C, respectively) greatly promoted their stability in water and transfection efficiency in vitro.

A number of cationic polymers have been developed to deliver exogenous genes into cells. Chitosan is a naturally occurring polysaccharide showing low cytotoxicity, biocompatibility, and biodegradability,[1] and is often employed as a gene carrier. Sato et al. reported that DNA/chitosan complexes were uptaken into tumor cells, but not into blood monocytes.[2] Plasmid DNA (pDNA)/chitosan also showed high-level transfection efficiency both in vitro[3] and in vivo.[4] However, the stability of pDNA/chitosan complexes in water was low by self-aggregation and BSA-induced aggregation. To improve the stability and cell-specificity of the pDNA complexes, lactose- and mannose-modified chitosans have been developed as gene carriers.[5]

Poly(ethylene glycol), PEG, has been widely employed for drug delivery systems to prevent non-specific interaction with serum protein and cells. Conjugation of PEG to pDNA/polyethyleneimine (PEI) complexes resulted in a prolonged circulation time after intravenous injection.[6] The conjugation of PEG to pDNA/chitosan complexes increased the stability in water.[7] However, such a conjugation of PEG to the pDNA/chitosan complexes did not enhance their transfection efficiency.

In this study, we employed PEG derivatives with carboxylic acid and sugar moieties (sugar–PEG-A/Cs) as side chains to coat DNA/chitosan complexes. Anionic sugar–PEG-A/Cs form ternary complexes electrostatically with cationic pDNA/chitosan complexes (Figure 1). Sugar–PEG-A/Cs have been employed to coat pDNA/PEI complexes and enhance transfection efficiency.[8] However, it has been reported that PEI induced strong cytotoxicity.[9] The toxicity of a pDNA/PEI complex was about seven times higher than that of a pDNA/chitosan complex.[10] Therefore, in this study, we prepared pDNA/chitosan/sugar–PEG-A/C ternary complexes and evaluated their transfection efficiency in vitro.

Chitosan was obtained from Yaizu Suisankagaku Industry (Shizuoka, Japan). The average molecular weight was 40000, and the degree of deacetylation was 85%. PEG-A/C and sugar–PEG-A/Cs were synthesized according to a previous paper.[8] The substitution degrees of maltose and lactose were 2.9 and 4.4 per molecule, respectively (Figure 1). The molecular weight of Mal–PEG-A/C was 9770, and that of Lac–PEG-A/C was

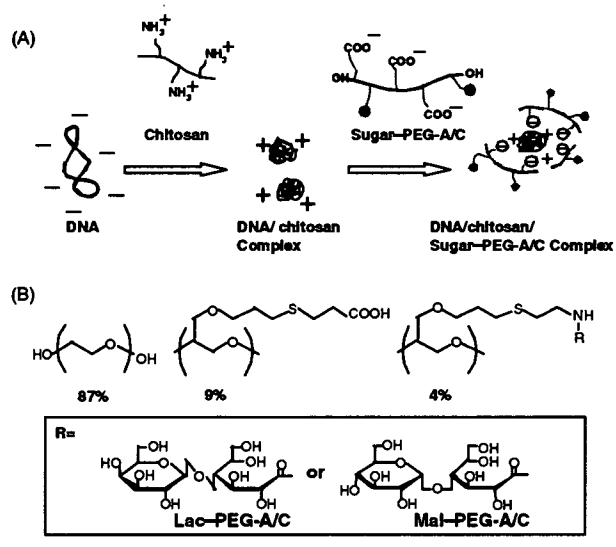

Figure 1. (A) A scheme for the formation of pDNA/chitosan/sugar–PEG-A/C ternary complexes. (B) Structure of sugar–PEG-A/Cs.

10300. A pDNA/chitosan complex was prepared according to the method previously reported.[3] The P/N ratio, which is the ratio of phosphate anion (P) of pDNA to the amino group (N) of chitosan, was 1/5. Ternary complexes were prepared by mixing preformed pDNA/chitosan complexes with aqueous solutions of PEG-A/C or sugar–PEG-A/Cs at appropriate P/N/C (C is carboxyl group of PEG-A/C) ratios for 15 min. In this study, pGL3-Luc (Promega) encoding the *luciferase* gene was employed as pDNA.

AFM observation with SPM-300 (Seiko Instruments Inc., Japan) indicated that the pDNA/chitosan complexes (P/N > 3) showed spherical structures of 200 nm in diameter. The morphology and size of the pDNA/chitosan/PEG-A/C complex at P/N/C = 1/5/20 were similar to the pDNA/chitosan complex. The particle size of the pDNA/chitosan/sugar–PEG-A/C complex was about 500 nm at N/P/C = 1/5/10 and 1/5/20. There was no obvious morphological difference between the pDNA/chitosan/Mal–PEG-A/C and pDNA/chitosan/Lac–PEG-A/C complexes.

The zeta potential was determined at various P/N/C ratios of the ternary complexes with a ZeeCom (Microtec Co., Ltd., Japan) at 25 °C (Figure 2). The zeta potential of the pDNA/chitosan complex at P/N = 1/5 was +49 mV, and was decreased by coating it with sugar–PEG-A/Cs. The zeta potentials of the pDNA/chitosan/sugar–PEG-A/C complexes were negative at P/N/C = 1/5/10 and 1/5/20. Therefore, it is considered that the surface of the cationic pDNA/chitosan complex was coated with anionic Mal–PEG-A/C and Lac–PEG-A/C.

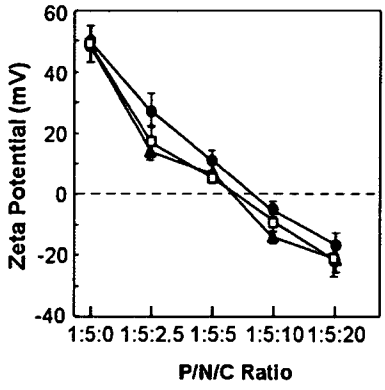

Figure 2. Zeta potentials of pDNA/chitosan/PEG-A/C (closed triangle), pDNA/chitosan/Mal–PEG-A/C (open square), and pDNA/chitosan/Lac–PEG-A/C (closed circle) complexes in 20 mM HEPES buffer. [pDNA] = 1.5 μg/mL.

The resistance of ternary complexes to degradation by DNaseI was investigated by agarose gel electrophoresis. The naked pDNA was completely digested by DNaseI (0.1 U) 50 mM Tris-HCl buffer containing 10 mM $MgCl_2$ and 100 mM NaCl at 37 °C for 30 min. On the other hand, the pDNA/chitosan and pDNA/chitosan/sugar–PEG-A/C complexes showed markedly improved resistance against DNaseI.

Luciferase activities of pDNA/chitosan/PEG-A/C complexes were investigated for B16 mouse melanoma cells. The transfection efficiency of the pDNA/chitosan/PEG-A/C complex at P/N/C = 1/5/2.5 decreased to one tenth that of the pDNA/chitosan complex. The transfection efficiencies of the ternary complexes were recovered by increasing the amount of PEG-A/C, and that of the complex of P/N/C = 1/5/40 was almost comparable with that of the pDNA/chitosan complex.

Next, the transfection efficiencies of the pDNA/chitosan/sugar–PEG-A/C complexes were investigated for B16 cells (Figure 3). The transfection efficiencies of pDNA/chitosan/

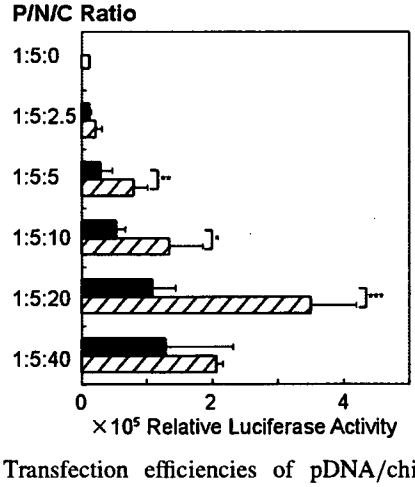

Figure 3. Transfection efficiencies of pDNA/chitosan/Lac–PEG-A/C (black bar) and pDNA/chitosan/Mal–PEG-A/C (cross-hatched bar) complexes at different P/N/C ratios. The luciferase activity of naked pDNA was normalized to 100. The luciferase activity of B16 cells transfected with 2.5 μg of pDNA per 2×10^5 cells represents the mean values of three experiments. The transfection time was 4 h, and post-transfection time was 20 h. * $P < 0.1$, ** $P < 0.05$, *** $P < 0.01$.

Lac–PEG-A/C and pDNA/chitosan/Mal–PEG-A/C complexes at P/N/C = 1/5/20 were 5.5- and 20-fold higher, respectively, than that of the pDNA/chitosan complex. The increased transfection efficiencies of the pDNA/chitosan/sugar–PEG-A/C complexes were also observed for human hepatoma HepG2 cells.

Since both the pDNA/chitosan/Lac–PEG-A/C and pDNA/chitosan/Mal–PEG-A/C complexes showed enhanced transfection efficiencies compared with pDNA/chitosan complexes, it was considered that physicochemical stability contributed to their high transfection efficiency. Thus, the interactions of the DNA complexes with anionic serum albumin and glycosaminoglycan (chondroitin sulfate) were investigated. The turbidity (at 350 nm) of the pDNA/chitosan complex markedly increased depending on the concentration of BSA (0.1–1 mg/mL), whereas those of the pDNA/chitosan/Mal–PEG-A/C complexes were significantly suppressed. Furthermore, the release of pDNA from the pDNA/chitosan and pDNA/chitosan/Mal–PEG-A/C complexes in the presence of 2% chondroitin sulfate was investigated by agarose gel electrophoresis. Though pDNA was released from the pDNA/chitosan complex, no release was observed from the pDNA/chitosan/Mal–PEG-A/C complex. These results suggested that the stability of the pDNA/chitosan complex against polyanions was improved by coating its surface with sugar–PEG-A/Cs. Improvement of the physicochemical stability of chitosan-containing gene carriers would be preferable for in vivo administration.

This work was partly supported by the Special Coordination of Funds for Promoting Science and Technology from the Ministry of Education, Culture, Sports, Science and Technology, Japan (T. S.).

References and Notes

1 S. Hirano, H. Seino, Y. Akiyama, I. Nonaka, *Polym. Eng. Sci.* **1988**, *59*, 897.
2 T. Sato, N. Shirakawa, H. Nishi, Y. Okahata, *Chem. Lett.* **1996**, 725.
3 a) T. Ishii, Y. Okahata, T. Sato, *Biochim. Biophys. Acta* **2001**, *1514*, 51. b) T. Sato, T. Ishii, Y. Okahata, *Biomaterials* **2001**, *22*, 2075.
4 a) K. Roy, H.-Q. Mao, S.-K. Huang, K. W. Leong, *Nature Med.* **1999**, *5*, 387. b) L. Illum, I. Jabbal-Gill, M. Hinchcliffe, A. N. Fisher, S. S. Davis, *Adv. Drug Delivery Rev.* **2001**, *51*, 81.
5 a) M. Hashimoto, M. Morimoto, H. Saimoto, Y. Shigemasa, T. Sato, *Bioconjugate Chem.* **2006**, *17*, 309. b) M. Hashimoto, M. Morimoto, H. Saimoto, Y. Shigemasa, H. Yanagie, M. Eriguchi, T. Sato, *Biotech. Lett.* **2006**, *28*, 815.
6 M. Ogris, S. Brunner, S. Schüller, R. Kircheis, E. Wagner, *Gene Ther.* **1999**, *6*, 595.
7 a) H.-Q. Mao, K. Roy, V. L. Troung-Le, K. A. Janes, K. Y. Lin, Y. Wang, J. T. August, K. W. Leong, *J. Controlled Release* **2001**, *70*, 399. b) I. K. Park, T. H. Kim, Y. H. Park, B. A. Shin, E. S. Choi, E. H. Chowdhury, T. Akaike, C. S. Cho, *J. Controlled Release* **2001**, *76*, 349.
8 Y. Koyama, E. Yamada, T. Ito, Y. Miautani, T. Yamaoka, *Macromol. Biosci.* **2002**, *2*, 251.
9 S. M. Moghimi, P. Symonds, J. C. Murray, A. C. Hunter, G. Debska, A. Szewczyk, *Mol. Ther.* **2005**, *11*, 990.
10 M. Köping-Höggård, I. Tubulekas, H. Guan, K. Edwards, M. Nilsson, K. M. Vårum, P. Artursson, *Gene Ther.* **2001**, *8*, 1108.
11 Supporting Information is available electronically on the CSJ-Journal Web site, http://www.csj.jp/journals/chem-lett.

Published on the web (Advance View) February 2, 2008; doi:10.1246/cl.2008.266

Available online at www.sciencedirect.com
ScienceDirect
Carbohydrate Research 343 (2008) 831–838
Carbohydrate RESEARCH

Glycosylation of dodecyl 2-acetamido-2-deoxy-β-D-glucopyranoside and dodecyl β-D-galactopyranosyl-(1→4)-2-acetamido-2-deoxy-β-D-glucopyranoside as saccharide primers in cells

Toshinori Sato,[a,*] Minako Takashiba,[a] Rumi Hayashi,[a] Xingyu Zhu[a] and Tatsuya Yamagata[b]

[a]*Department of Biosciences and Informatics, Keio University, Yokohama 223-8522, Japan*
[b]*Shenyang Pharmaceutical University, PO Box 29, School of Pharmaceutical Engineering, Shenyang 110016, PR China*

Received 3 July 2007; received in revised form 26 December 2007; accepted 16 January 2008
Available online 26 January 2008

Abstract—Syntheses of oligosaccharides expressed on cells are indispensable for the improvement of the functional analyses of the oligosaccharides and their applications. We are developing saccharide primers for synthesizing oligosaccharides using living cells. In this study, dodecyl 2-acetamido-2-deoxy-β-D-glucopyranoside (GlcNAc-C12) and dodecyl β-D-galactopyranosyl-(1→4)-2-acetamido-2-deoxy-β-D-glucopyranoside (LacNAc-C12) were examined for their abilities to prime the syntheses of neolacto-series oligosaccharides in HL60 cells. When GlcNAc-C12 was incubated with HL60 cells in serum-free medium for 2 days, 14 kinds of glycosylated products were collected from the culture medium. They were separated by high-performance liquid chromatography. The sequences of the products were determined to be neolacto-series oligosaccharides including Lewis^X, sialyl Lewis^X, polylactosamine, and sialylpolylactosamine by mass spectrometry. GlcNAc-C12 was also glycosylated by B16 cells and gave sialyllactosamine. Furthermore, LacNAc-C12 gave similar glycosylated products to GlcNAc-C12.

Keywords: Saccharide primer; *N*-Acetylglucosamine; *N*-Acetyllactosamine; Oligosaccharide; Glycosylation; Animal cells

1. Introduction

The importance of technology to synthesize oligosaccharides expressed on mammalian cells has been indicated by the elucidation of their roles in cell function. We have been developing saccharide primer methods to synthesize oligosaccharides using the glycan biosynthesis system in cells. A saccharide primer is a glycolipid analogue to be glycosylated by cells in culture. Yamagata and co-workers have developed amphiphilic glycolipid analogues such as alkyllactosides.[1,2] Dodecyl β-lactoside (Lac-C12) as a saccharide primer was incorporated into B16 melanoma cells and was glycosylated by glycosyltransferase. The glycosylated product was secreted from the cells. Structural analyses indicated that the product was sialyllactose, which is the carbohydrate portion of GM3 normally expressed on the surface of mouse B16 melanoma cells.

Other primers as substrates for glycosyltransferase in cells have been described in several reports. β-D-Xylosides have been developed as an initiator of glycosaminoglycan biosynthesis.[3,4] Acetylated Xylβ1-6Gal-*O*-2-naphthol and acetylated Galβ1-4GlcNAcβ-*O*-naphthalenemethanol (NM) were investigated as inhibitors of the glycosyltransferase in cells.[5] Furthermore, acetylated Galβ1-4GlcNAcβ-NM and acetylated GlcNAcβ1-3Galβ-NM inhibited the biosynthesis of endogenous sialyl Lewis^X, and they were also glycosylated in human promyelocytic leukemia HL60 cells.[6]

The glycosylation of the saccharide primers was suggested to be dependent on the cell lines, because different types of cells have different intrinsic glycan biosynthesis

* Corresponding author. Tel.: +81 45 566 1771; fax: +81 45 566 1447; e-mail: sato@bio.keio.ac.jp

0008-6215/$ - see front matter © 2008 Elsevier Ltd. All rights reserved.
doi:10.1016/j.carres.2008.01.022

systems. Therefore, a saccharide library could be synthesized by combining various saccharide primers and cells. HL60 cells are known to express ganglioside GM3 and neolacto-series oligosaccharides. When Lac-C12 was incubated with HL60 cells, only the sialylated product (sialyllactose) was obtained, but not neolacto-series oligosaccharides. Therefore, in the present study, we synthesized dodecyl 2-acetamido-2-deoxy-β-D-glucopyranoside (GlcNAc-C12) and dodecyl β-D-galactopyranosyl-(1→4)-2-acetamido-2-deoxy-β-D-glucopyranoside (LacNAc-C12) as saccharide primers (Fig. 1), and the glycosylation reactions of those primers by HL 60 cells and B16 cells were examined.

2. Results

2.1. Glycosylation of GlcNAc-C12 by HL60 cells

HL60 cells were employed to examine the usefulness of GlcNAc-C12 as saccharide primer for the synthesis of neolacto-series oligosaccharides. After incubation of 50 μM of GlcNAc-C12 with HL60 cells, glycosylated products and unreacted primers were collected from the culture medium and cell fraction using a Sep-Pak C_{18} column. The glycosylated products adsorbed to the column were eluted using mixed solvents of methanol and water. The glycosylated products were largely detected from the culture medium. The acidic and neutral products were eluted with 3:7 MeOH–H_2O, and 1:9 MeOH–H_2O, respectively. As shown in Figure 2A, HPTLC (high-performance thin-layer chromatography) indicated that the fractions eluted with 3:7 MeOH–H_2O contained four neutral products (N1–N4), and the fractions eluted with 1:9 MeOH–H_2O contained six acidic products (A1–A6). Next, the neutral and acidic products were separated by high-performance liquid chromatography (HPLC). The four neutral products were separated using 70:28:2 $CHCl_3$–MeOH–H_2O as shown in Figure 2B. N1, N2, N3, and N4 were detected in fraction numbers 7–9, 11–12, 35–40, and 70–80, respectively. The four acidic products (A1–A4) were separated using 70:28:2 $CHCl_3$–MeOH–H_2O as shown in Figure 2C. A1, A2, A3, and A4 were detected in fraction numbers 17–19, 20–23, 26–28, and 45–50, respectively. Two acidic products (A5–A6) were separated using 60:35:5 $CHCl_3$–MeOH–H_2O as shown in Figure 2D. A4 and A5 were detected in fraction numbers 10 and 11–13, respectively.

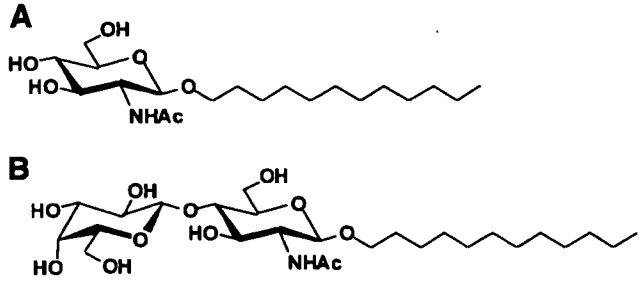

Figure 1. Saccharide primers, GlcNAc-C12 (A) and LacNAc-C12 (B), employed in this study.

2.2. Analyses of the chemical structures of products by mass spectrometry

Analyses of the structures of products separated by HPLC were carried out by MALDI-TOFMS (matrix-assisted laser desorption and ionization time-of-flight mass spectrometry). The observed masses and the deduced sequences of the glycosylated products are shown in Table 1. The mobility of N1 on HPTLC was same as that of synthetic Galβ1-4GlcNAc-C12 (LacNAc-C12), and the non-reducing hexose of N1 was cleaved by jack bean β-galactosidase (data not shown). Furthermore, the positive MALDI-PSD (post-source decay)

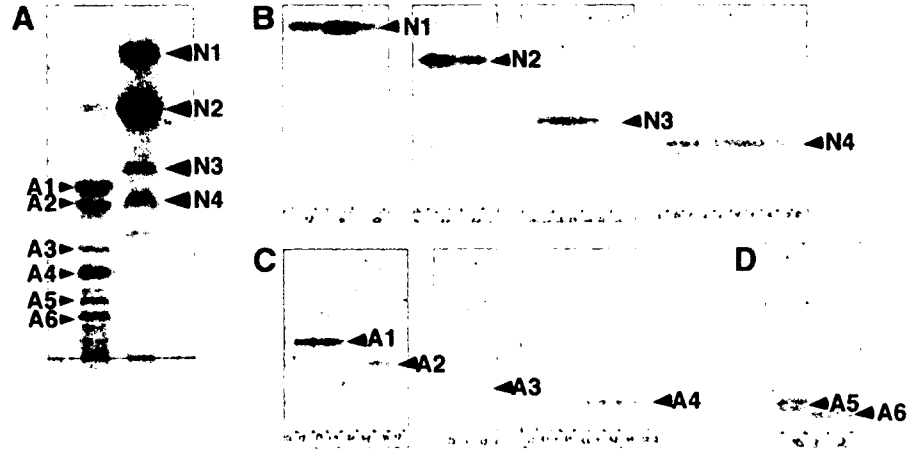

Figure 2. HPTLC of the products collected using a Sep-Pak C_{18} column (A), and purified by HPLC (B, C, and D) for the glycosylation of GlcNAc-C12 by HL60 cells.

Table 1. Deduced sequences and mass observed by MALDI-TOF-MS for the glycosylated products from GlcNAc-C12

Product	Sequence	Observed mass
N1	Galβ1-4GlcNAc-C12	574.1 $[M+Na]^+$
N2	Galβ1-4(Fucα1-3)-GlcNAc-C12	720.1 $[M+Na]^+$
N3	Galβ1-4GlcNAcβ1-3Galβ1-4GlcNAc-C12	939.1 $[M+Na]^+$
N4	Galβ1-4GlcNAcβ1-3Galβ1-4(Fucα1-3)GlcNAc-C12	1085.3 $[M+Na]^+$
A1	NeuNAcα2-3Galβ1-4GlcNAc-C12	841.4 $[M-H]^-$
A2	NeuNAcα2-6Galβ1-4GlcNAc-C12	841.4 $[M-H]^-$
A3	NeuNAc-(Galβ1-4GlcNAc)$_2$-C12	1230.1 $[M-H]^-$
A4	Fucose+A3	1376.3 $[M-H]^-$
A5	NeuNAc-(Galβ1-4GlcNAc)$_3$-C12	1595.9 $[M-H]^-$
A6	Fucose+A5	1742.0 $[M-H]^-$

spectrum (Table 2) revealed a peak at *m/z* 305.32 corresponding to $^{0,2}A_2$ fragment ($+Na^+$, intramolecular cleavage of GlcNAc). The results of MALDI-PSD agreed with the values in the literature.[7] Thus, N1 was determined to be Galβ1-4GlcNAc-C12. N2 was predicted to be H antigen (Fuc-Gal-GlcNAc-C12) or Lewis^X (Gal-(Fuc)-GlcNAc-C12) from the peak of *m/z* 720.1 ($[M+Na]^+$) of the MALDI-TOF-MS spectrum (Table 1). The MALDI-PSD spectrum of N2 (Table 2) revealed peaks at *m/z* 558.4 corresponding to $Y_{1\beta}$ (Fuc-GlcNAc-C12+Na^+) and *m/z* 305.4 corresponding to the $Y_{1\alpha}/^{0,2}A_2$ fragment ($+Na^+$). The observed fragment ions of N2 were similar to the MALDI-PSD spectrum of Lewis^X reported in the literature.[7] Therefore, N2 was determined to be Lewis^X. N3 was predicted to be Gal-GlcNAc-Gal-GlcNAc-C12 from the peak of *m/z* 939.1 ($[M+Na]^+$) of the MALDI-TOF-MS spectrum (Table 1). The MALDI-PSD spectrum of N3 (Table 2) revealed peaks at *m/z* 670.5 corresponding to $^{0,2}A_4$ fragment ($+Na^+$) and *m/z* 305.3 corresponding to $^{0,2}A_2$ fragment ($+Na^+$), suggesting the existence of two β-(1→4) lactosamine units. N4 was predicted to be fucosylated N3 from the peak of *m/z* 1085.3 ($[M+Na]^+$) of the MALDI-TOF-MS spectrum (Table 1). The MALDI-PSD spectrum of N4 (Table 2) revealed a peak at *m/z* 558.6 corresponding to $Y_{1\beta}$ (Fuc-GlcNAc-C12+Na^+), and fragmentation ions were similar to those of N3, suggesting that N4 is Galβ1-4GlcNAcβ1-3Galβ1-4(Fucα1-3)GlcNAc-C12. HL60 cells express FUT4, which transfers fucose to lactosamine.[8] Furthermore, it has been reported that FUT4 preferentially transfers fucose to inner GlcNAc residues.[9] The structure of N5 agreed with that of the endogenous glycan reported in the literature.[8,9]

Though the mobilities of A1 and A2 on HPTLC were different, the MALDI-TOF-MS spectra of them revealed the same mass of 841.4 ($[M-H]^-$), corresponding to NeuNAc-Gal-GlcNAc-C12 (sLacNAc-C12, Table 1). Since A1 and A2 are considered to have different linkages of *N*-acetylneuraminic acid to galactose, the

Table 2. Fragment ions observed by MALDI-PSD spectrum for the glycosylated products from GlcNAc-C12

Product	Fragments
N1	226.4 ($[Y_1/B_2+Na]^+$), 305.3 ($[^{0,2}A_2+Na]^+$), 388.4 ($[B_2+Na]^+$), 412.4 ($[Y_1+Na]^+$),
N2	226.3 ($[Y_{1\alpha}/Y_{1\beta}/B_2+Na]^+$), 305.4 ($[Y_{1\alpha}/^{0,2}A_2+Na]^+$), 370.5 ($[Z_1/B_2+Na]^+$), 388.3 ($[Y_{1\alpha}/B_2+Na]^+$), 412.4 ($[Y_{1\alpha}/Y_{1\beta}+Na]^+$), 534.4 ($[B_2+Na]^+$), 556.4 ($[Z_1+Na]^+$), 558.4 ($[Y_{1\beta}+Na]^+$), 574.6 ($[Y_{1\alpha}+Na]^+$)
N3	226.3 ($[Y_3/B_2+Na]^+$, $[B_4/Y_1+Na]^+$), 305.3 ($[^{0,2}A_2+Na]^+$), 388.2 ($[B_2+Na]^+$ or $[B_4/Y_2+Na]^+$), 406.4 ($[C_2+Na]^+$), 412.5 ($[Y_1+Na]^+$), 550.3 ($[B_3+Na]^+$), 574.5 ($[Y_2+Na]^+$), 670.5 ($[^{0,2}A_4+Na]^+$), 753.7 ($[B_4+Na]^+$), 777.9 ($[Y_3+Na]^+$)
N4	226.4 ($[Y_3/B_2+Na]^+$, $[Y_{1\alpha}/B_4/Y_{1\beta}+Na]^+$), 305.3 ($[^{0,2}A_2+Na]^+$), 388.5 ($[B_2+Na]^+$ or $[Y_{1\alpha}/B_4/Y_2+Na]^+$), 406.5 ($[C_2+Na]^+$), 412.7 ($[Y_{1\alpha}/Y_{1\beta}+Na]^+$), 550.6 ($[B_3+Na]^+$), 558.7 ($[Y_{1\beta}+Na]^+$), 574.9 ($[Y_{1\alpha}/Y_2+Na]^+$), 670.4 ($[Y_{1\alpha}/^{0,2}A_4+Na]^+$), 720.6 ($[Y_2+Na]^+$), 778.0 ($[Y_{1\alpha}/Y_3+Na]^+$), 901.9 ($[Y_3+Na]^+$), 940.0 ($[Y_{1\alpha}+Na]^+$)
A3	388.3 ($[Y_4/B_3+Na]^+$, $[Y_2/B_5+Na]^+$), 406.5 ($[Y_4/C_3+Na]^+$), 412.4 ($[Y_1+Na]^+$), 476.3 ($[B_2+Na]^+$), 550.5 ($[Y_4/B_4+Na]^+$), 574.6 ($[Y_2+Na]^+$), 634.9 ($[^{0,2}A_3+Na+K-H]^+$), 679.6 ($[B_3+Na]^+$), 753.8 ($[B_5/Y_3+Na]^+$), 777.7 ($[Y_3+Na]^+$), 939.8 ($[Y_4+Na]^+$)
A4	336.4 ($[B_1+2Na-H]^+$), 388.4 ($[Y_4/B_3+Na]^+$ or $[Y_{1\alpha}/Y_2/B_5+Na]^+$), 406.5 ($[Y_4/C_3+Na]^+$), 412.3 ($[Y_{1\alpha}/Y_{1\beta}+Na]^+$), 476.5 ($[B_2+Na]^+$), 550.6 ($[Y_4/B_4+Na]^+$), 558.9 ($[Y_{1\beta}+Na]^+$), 574.6 ($[Y_{1\alpha}/Y_2+Na]^+$), 634.9 ($[^{0,2}A_3+Na+K-H]^+$), 679.6 ($[B_3+Na]^+$), 720.9 ($[Y_2+Na]^+$), 777.8 ($[Y_{1\alpha}/Y_3+Na]^+$), 841.3 ($[B_4+Na]^+$), 923.9 ($[Y_3+Na]^+$), 939.6 ($[Y_{1\alpha}/Y_4+Na]^+$), 1085.4 ($[Y_4+Na]^+$), 1230.8 ($Y_{1\alpha}$)
A5	388.1 ($[Y_6/B_3+Na]^+$, $[B_5/Y_4+Na]^+$ or $[B_7/Y_2+Na]^+$), 406.2 ($[Y_6/C_3+Na]^+$ or $[C_5/Y_4+Na]^+$), 550.3 ($[B_6/Y_4+Na]^+$), 574.6 ($[Y_2+Na]^+$), 591.2 ($[Y_5/B_5+Na]^+$ or $[B_7/Y_4+Na]^+$), 596.7 ($[^{0,2}A_3+Na]^+$), 634.9 ($[^{0,2}A_3+Na+K-H]^+$), 670.2 ($[Y_6/^{0,2}A_5+Na]^+$, $[Y_4/^{0,2}A_7+Na]^+$), 679.5 ($[B_3+Na]^+$), 753.6 ($[Y_6/B_5+Na]^+$ or $[B_7/Y_4+Na]^+$), 777.6 ($[Y_3+Na]^+$), 916.8 ($[Y_4+H]^+$), 939.5 ($[Y_4+Na]^+$), 999.8 ($[^{0,2}A_5+Na]^+$), 1045.1 ($[B_5+Na]^+$), 1142.7 ($[Y_5+Na]^+$), 1305.0 ($[Y_6+Na]^+$)
A6	388.6 ($[Y_6/B_3+Na]^+$, $[B_5/Y_4+Na]^+$ or $[Y1_\alpha/B_7/Y_2+Na]^+$), 406.8 ($[Y_6/C_3+Na]^+$, $[C_5/Y_4+Na]^+$), 550.5 ($[B_6/Y_4+Na]^+$), 574.9 ($[Y_{1\alpha}/Y_2+Na]^+$), 591.3 ($[Y_5/B_5+Na]^+$ or $[Y_{1\alpha}/B_7/Y_3+Na]^+$), 596.2 ($[^{0,2}A_3+Na]^+$), 634.4 ($[^{0,2}A_3+Na+K+H]^+$), 720.2 ($[Y_2+Na]^+$), 753.8 ($[Y_{1\alpha}/Y_6/^{0,2}A_5+Na]^+$ or $[Y_{1\alpha}/Y_4/^{0,2}A_7+Na]^+$), 777.6 ($[Y_{1\alpha}/Y_3+Na]^+$), 899.9 ($[Y_4/B_7+Na]^+$), 916.9 ($[Y_{1\alpha}/Y_4+H]^+$), 923.9 ($[Y_3+Na]^+$), 939.8 ($[Y_{1\alpha}/Y_3+Na]^+$), 1000.0 ($[Y_{1\alpha}/^{0,2}A_5+Na]^+$), 1045.5 ($[B_5+Na]^+$), 1085.7 ($[Y_4+Na]^+$), 1288.8 ($[Y_5+Na]^+$), 1304.5 ($[Y_{1\alpha}/Y_6+Na]^+$), 1451.0 ($[Y_6+Na]^+$), 1472.6 ($[Y_6+2Na-H]^+$), 1596.1 ($[Y_{1\alpha}+Na]^+$)